Thermodynamic pathways to melting, ablation, and solidification in absorbing solids under pulsed laser irradiation

Patrick Lorazo,[1,2] Laurent J. Lewis,[2,*] and Michel Meunier[1,†]
[1]*Laboratoire de Procédés par Laser, Département de Génie Physique, École Polytechnique de Montréal, C.P. 6079, Succursale Centre-Ville, Montréal (Québec), Canada H3C 3A7*
[2]*Département de Physique et Regroupement Québécois sur les Matériaux de Pointe (RQMP), Université de Montréal, C.P. 6128, Succursale Centre-Ville, Montréal (Québec), Canada H3C 3J7*
(Received 11 October 2005; revised manuscript received 23 February 2006; published 14 April 2006)

The thermodynamic pathways involved in laser irradiation of absorbing solids are investigated in silicon for pulse durations of 500 fs and 100 ps. This is achieved by accounting for carrier and atom dynamics within a combined Monte Carlo and molecular-dynamics scheme and simultaneously tracking the time evolution of the irradiated material in ρ-T-P space. Our simulations reveal *thermal* changes in long-range order and state of aggregation driven, in most cases, by *nonequilibrium* states of rapidly heated or promptly cooled matter. Under femtosecond irradiation near the ablation threshold, the system is originally pulled to a near-critical state following rapid ($\lesssim 10^{-12}$ s) disordering of the *mechanically unstable* crystal and isochoric heating of the resulting metallic liquid. The latter is then adiabatically *cooled* to the liquid-vapor regime where phase explosion of the subcritical, *superheated* melt is initiated by a direct conversion of translational, *mechanical* energy into surface energy on a $\sim 10^{-12}$–10^{-11} s time scale. At higher fluences, matter removal involves, instead, the fragmentation of an initially homogeneous fluid subjected to large strain rates upon rapid, *supercritical* expansion in vacuum. Under picosecond irradiation, homogeneous and, at later times, heterogeneous melting of the superheated solid are followed by nonisochoric heating of the molten metal. In this case, the *subcritical* liquid material is subsequently cooled onto the binodal by thermal conduction and explosive boiling does *not* take place; as a result, ablation is associated with a "trivial" fragmentation process, i.e., the relatively slow expansion and dissociation into liquid droplets of *supercritical* matter *near thermodynamic equilibrium*. This implies a liquid-vapor equilibration time of $\sim 10^{-11}$–10^{-10} s and heating *along* the binodal under nanosecond irradiation. Solidification of the nonablated, *supercooled* molten material is eventually observed on a $\sim 10^{-11}$–10^{-9} s time scale, irrespective of the pulse duration.

DOI: 10.1103/PhysRevB.73.134108 PACS number(s): 79.20.Ds, 79.20.Ap, 61.80.Az

I. INTRODUCTION

Pulsed laser irradiation of solids, i.e., the interaction of relatively short ($\sim 10^{-13}$–10^{-8} s), intense ($\sim 10^{9}$–10^{14} W cm^{-2}) bursts of coherent and monochromatic light with surfaces, offers a unique way to perturb materials away from equilibrium:[1–7] here, absorption of the photons by the valence- and conduction-band electrons sets the initial stage for a complex chain of events covering multiple length (electronic to macroscopic) and time (femtosecond to microsecond) scales.[8] In some cases, changes in the long-range order and/or state of aggregation of the material are involved: examples of structural modifications include direct solid-solid,[9] solid-liquid,[10–12] and liquid-gas[13–17] transitions. These, in turn, have been extensively exploited for laser processing of materials: applications range from surface micromachining,[18] cleaning,[19] and annealing[20] to thin-film growth[21,22] and the production of nanoparticles in vacuum[23,24] and aqueous solutions;[25] lasers have also found extensive use in medicine and surgery for the manipulation and destruction of biological tissues.[26]

The nature of the phenomena induced by laser radiation in transparent (insulators or dielectrics) and absorbing (metals and semiconductors) solids is determined, for the most part, by the coupling of the laser parameters—pulse duration τ_L, wavelength λ_L, and energy per unit area (fluence) F—with the optical, mechanical, and thermal properties of the material. In general, the absorption of a laser pulse gives rise to a gas of hot carriers (electrons or electron-hole pairs at a temperature T_e) which, through repeated emission of phonons, heat the initially cooler ions (at a temperature T) to achieve a common equilibrium after $\tau_E \sim 10^{-12}$–10^{-11} s.[27] This time scale has far-reaching significance. It sets a boundary between strictly thermal and possible nonthermal routes, a dividing line between "long" and "short" pulses:[28] if $\tau_L \gg \tau_E$, equilibrium between electrons and phonons prevails throughout the heating stage ($T_e \approx T$) and phase change can usually be regarded as a slow thermal process involving quasiequilibrium thermodynamic states; examples under nanosecond laser irradiation include *heterogeneous* melting[29,30] and, at higher fluences, vaporization[17] at moving solid-liquid and liquid-vacuum boundaries, respectively. Under ultrashort pulses ($\tau_L \lesssim 10^{-12}$ s), however, the material is left in a highly nonequilibrium state following the deposition of the optical energy ($T_e \gg T$):[31] in this case, the time with which a given structural modification takes place, τ_M, determines whether thermal mechanisms are involved ($\tau_M \gg \tau_E$) or not ($\tau_M < \tau_E$).[28] In certain circumstances, there may be enough time to establish electron-phonon equilibrium but insufficient time to achieve *phase* equilibrium between the different states of aggregation ($\tau_M \approx \tau_E$):[32] here, transient, *nonequilibrium* states associated with the *homogeneous* nucleation of critical

nuclei of liquid or gas in a metastable, superheated solid,[33–36] or liquid,[13–15,37,38] respectively, are likely to take part in rapid, thermal phenomena. The occurrence of long lived, supercooled states in the melt prior to crystallization or amorphization have also been reported for pulses of femtosecond to nanosecond duration.[11,39–42]

The existence of competing thermal and nonthermal channels in order-to-disorder transitions is exemplified in ultrashort-pulse laser melting of several semiconductors including indium antimonide,[3] germanium,[5,10] gallium arsenide,[43–45] and silicon.[45–47] On the one hand, if a threshold number of strong, directional, covalent bonds are broken or, equivalently, if the number of electrons that have been promoted from bonding (valence) to antibonding (conduction) states reaches a critical density $N_c \approx 10^{22}$ cm^{-3},[48,49] the tetravalent lattice collapses to a sixfold-coordinated[50] metallic liquid on a subpicosecond time scale, i.e., *before* carrier-phonon equilibration is achieved. At lower excitations, on the other hand, the path from solid to liquid is presumably a rapid, picosecond, thermal process, i.e., slower than ultrafast nonthermal disordering but significantly faster than heterogeneous, surface-nucleated melting.[33,34] In this case, the transition to the molten state likely proceeds by homogeneous nucleation of liquid inclusions in the strongly superheated, metastable, bulk crystal.[51]

The removal of macroscopic amounts of matter at a laser-irradiated surface, i.e., laser ablation, reveals an additional battleground where thermal and nonthermal pathways collide. In transparent materials, on the one hand, high intensities commonly delivered by femtosecond pulses are normally required to excite electrons across the large band gap:[52] here, multiphoton ionization provides the initial seed electrons which later gain kinetic energy from the laser radiation to produce additional free carriers through an impact ionization, avalanche process. At irradiances above a threshold $I_{\text{break}} \sim 10^{13}$ W cm^{-2}, a direct solid-to-plasma transition follows by optical breakdown:[28,53–55] the dielectric material is fully ionized into a very dense ($N \sim 10^{23}$ cm^{-3}) and hot ($T_e \sim 10^6$ K) plasma which is rapidly carried away with a velocity of $\sim 10^4 - 10^5$ m s^{-1}. Ablation following loss of charge neutrality and ion repulsion at the surface has also been reported.[56–59]

In absorbing materials, on the other hand, strong single-photon coupling of the laser field with the solid makes matter removal also achievable with femtosecond,[13,28,32,38,54,60] picosecond,[60–63] and nanosecond[17,60,64–66] pulses at irradiances well below I_{break}.[67] In this case, significantly lower temperatures ($\sim 10^3 - 10^4$ K) and ejection velocities ($\sim 10^2 - 10^3$ m s^{-1}) reveal a strictly *thermal* ejection pathway belonging to either one or the other of the following two broad classes of mechanisms:[68] (i) *Photothermal* processes in which changes in the state of aggregation of the molten material arise from a first- (or possibly second-) order phase transition to a vapor; possible outcomes include homogeneous nucleation of gas bubbles in a metastable liquid, i.e., phase explosion or explosive boiling,[13,15,62,64–66,69–77] phase separation of a mechanically unstable liquid by spinodal decomposition,[72,78] and normal vaporization at the outer surface.[17,74,79] (ii) *Photomechanical* processes in which the breakup of the material is assisted by strong, tensile pressure waves—spallation[71,73,80] in solids and cavitation[81,82] in liquids—or involves the dissociation of a homogeneous, supercritical fluid into clusters upon dilution in vacuum, i.e., fragmentation.[73–77,83]

In order to explain ablation in metals irradiated by long (nanosecond) pulses, Miotello and Kelly,[70,84] following previous work by Martynyuk,[69,85,86] have proposed a picture in which matter removal results from a phase-explosion process. The scenario, further put forward by numerous authors for femtosecond,[72,87] picosecond,[61,62,71,88] and nanosecond[64–66] pulses, can be outlined as follows: (i) If $\tau_L \gg \tau_{\text{LV}}$—where, according to Ref. 64, $\tau_{\text{LV}} \sim 10^{-9} - 10^{-8}$ s is the time required for a metallic liquid to achieve equilibrium with its vapor—the expanding molten material is stable and heating takes place along the liquid-vapor coexistence (saturation) line, i.e., the binodal. If $\tau_L \lesssim \tau_{\text{LV}}$, however, a significant fraction of the energy is stored in the metallic melt before it can be consumed as latent heat of vaporization. In this case, the liquid attempts to equilibrate with its undersaturated vapor and its heating line lies, instead, below the binodal: the liquid is pushed into the liquid-gas regime as it is *rapidly heated*.[62,64,65,84,85] (ii) If the fluence is sufficiently high, the molten metal is superheated near the spinodal[89] (the limit of mechanical stability) to a temperature of $\approx 0.9T_c$ (where T_c is the thermodynamic critical temperature).[64,65,69,70] (iii) Nucleation and growth of gas bubbles sets in on a time scale[69,70,85,86,90] $\tau_{\text{NUC}} \sim 10^{-9} - 10^{-7}$ s and the metastable mother phase is converted into a heterogeneous mixture of liquid and gas, i.e., explosive boiling occurs. The threshold nature of the ablation process, evidenced by (iv) the sharp increase in the total ablated mass[38,66,91,92] and (v) the onset of large, nanometer-to micron-sized, liquid-droplet ejection[66,93] at a well-defined fluence F_{abl}, has often been ascribed to an abrupt rise in the bubble nucleation rate as the metastable liquid is heated toward the spinodal limit.[64,65,70,71,94–96]

However, ultrafast time-resolved microscopy experiments[13,32,38,54] have suggested, and various analytical[15,37,97] and molecular-dynamics[14,73–77] calculations confirmed, that the thermal routes to ablation in absorbing solids embrace a fundamentally different, universal behavior under femtosecond laser irradiation: (i) Here, the material is initially pulled *away* from the liquid-vapor regime to a near-critical or supercritical state upon rapid, isochoric heating; the metastable region is approached, instead, as the pressurized matter adiabatically *cools* during its subsequent dilution in vacuum. (ii) In a relatively narrow range of fluences close to the ablation threshold ($1 \lesssim F/F_{\text{abl}} \lesssim 1.5$ in Si),[38,98] expansion takes place along subcritical isentropes until the binodal is reached; very near F_{abl}, the latter is crossed at a temperature which may lie significantly below $0.9T_c$.[76,77] (iii) As a result of homogeneous nucleation of a stable vapor phase in the metastable liquid phase, on the one hand, and a sharp drop of the sound velocity giving rise to a steep ablation front, on the other hand, the expanding material subsequently develops a bubblelike structure on a $10^{-12} - 10^{-11}$ s time scale:[13,74,76] a low-density, heterogeneous, two-phase mixture between two optically flat, reflective interfaces—the nonablated matter and a thin, moving liquid shell—is expelled from the surface through a phase-explosion process. The ob-

servation of interference fringes (Newton rings) during time-resolved femtosecond laser excitation and imaging of numerous metal and semiconductor surfaces supports this scenario.[13,32,38,54]

Upon increasing the fluence, before the onset of plasma formation in semiconductors ($1.5 \lesssim F/F_{abl} \lesssim 3$ in Si),[38,98] the density profile smooths out and the interference pattern eventually vanishes as the diluting material shifts from a subcritical liquid to a supercritical fluid. In this case, fragmentation gradually takes over explosive boiling as the primary pathway to matter removal.[73,74,77,83]

Under picosecond laser irradiation, however, expansion is slower and cooling is nonadiabatic:[75–77] the expanding subcritical material is efficiently cooled onto the binodal by thermal conduction and phase explosion does not take place; here, the onset of (iv) ablation and (v) droplet ejection is determined, rather, by the breakup of a hot, supercritical fluid near thermodynamic equilibrium, i.e., "trivial" fragmentation. This points to a shorter liquid-vapor equilibration time $\tau_{LV} \sim 10^{-11}-10^{-10}$ s and, consequently, a heating process *along* the binodal under nanosecond pulses.

In spite of recent advances, a thorough understanding of the changes in long-range order and state of aggregation induced in solids by laser radiation has yet to come. From a thermodynamic standpoint, the transient, superheated, and supercooled states involved in, e.g., the rapid melting and solidification of the irradiated material, respectively, are difficult to assess experimentally. From a kinetic viewpoint, the dynamics of void nucleation and the puzzling nature of the ablation threshold under pulsed laser irradiation can directly be addressed at atomic-to-mesoscopic scales by computational means.

In this paper, which follows preliminary results presented in Refs. 76 and 77, we report on the structural modifications induced in silicon by 500 fs and 100 ps laser pulses. We explore the *thermal* regime where the laser field acts as a fast heat source and the heated material obeys the laws of thermodynamics and hydrodynamics of fluids. As detailed in Sec. II, this is achieved on a nanosecond time scale by coupling carrier and atom dynamics within a combined Monte Carlo (MC) and molecular-dynamics (MD) scheme, and simultaneously pursuing the time evolution of the irradiated matter in density-temperature-pressure (ρ-T-P) space during heating, expansion, and cooling. The thermal pathways observed in the femtosecond and picosecond regimes are discussed in Secs. III and IV, respectively: in each case, the routes to melting, ablation, and solidification are identified; in particular, the nature of the ablation threshold under ultrashort-pulse irradiation is carefully examined in Sec. III C. A unified picture of the thermodynamic pathways available to the irradiated material under femtosecond to nanosecond pulses finally emerges in Sec. IV C.

II. COMPUTATIONAL SCHEME

A. Combined MC and MD model

A schematic illustration of the model is displayed in Fig. 1. We give here a rapid overview of its most important features; full details are provided in Secs. II A 1 to II A 4.

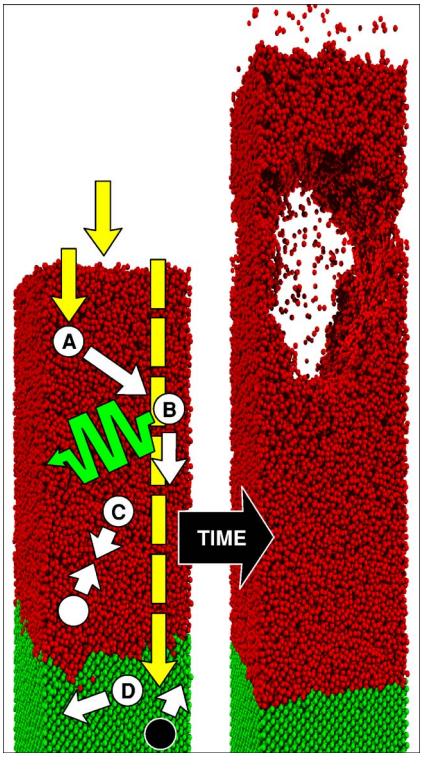

FIG. 1. (Color online) Schematic view of the combined MC and MD model for silicon. Left: absorption of the photons and carrier scattering processes. Right: growth of a relatively large cavity prior to the ejection of hot, molten material. Red spheres: atoms belonging to the (metallic) liquid phase; green spheres: atoms belonging to the (semiconducting) crystalline phase; yellow arrows: photons; white disks: conduction electrons; black disk: conduction hole; green wavy arrow: phonon; white arrows: carrier motion (direction and velocity). Capital letters refer to specific absorption and scattering events. See text for full details.

In most cases of interest to the present study, part of the silicon target melts during the pulse. As a result, a significant number of photons (yellow arrows) incident along the z axis (normal to the initial surface) are absorbed by conduction electrons (white disks) in the *metallic* liquid layer (red atoms) at the surface (marked A); if ablation takes place, absorption may also occur in the expanding plume (see Sec. II A 1). The deposited energy is subsequently shared among other carriers and ions: in accordance with a standard MC procedure, the Drudelike carriers undergo ballistic transport between two successive collisions which instantaneously change their velocity and energy but not their position. Upon emission of a phonon (green wavy arrow), an electron is scattered in a new direction (chosen at random) with a velocity reduced in a way that reflects the corresponding loss of kinetic energy, cf. change in orientation and length of the white arrow (B); other collisions in the melt involve energy exchange upon carrier-carrier scattering (C). In the crystalline, semiconducting bulk (green atoms), the absorption of a photon usually leads to the creation of an electron and hole (black disk) with different initial velocities and energies (D); collisional processes include scattering with carriers and phonons, Auger recombination, and impact ionization (not

shown). Atom dynamics are treated using classical MD: depending on the fluence, melting of the silicon crystal, ejection of liquid material, and solidification of the nonablated, molten matter may take place on mesoscopic-length and picosecond-to-nanosecond-time scales. We expect that the general features of our model also apply to other group IV (as well as III–V) semiconductors, also characterized by a metallic liquid phase.

1. Laser pulse and absorption processes

The laser pulse having a duration $\tau_L=500$ fs or 100 ps full width at half maximum (FWHM) and a wavelength $\lambda_L=266$ nm is Gaussian in time but spatially uniform. It is modeled by successive groups of photons with energy $\hbar\omega_L=4.66$ eV which couple to "carriers" over a penetration depth of $\approx 5-10$ nm (in both *c*-Si and *l*-Si). As briefly mentioned above and detailed below, a carrier is a particle (electron or hole) which follows Drude dynamics while undergoing various scattering events, each with its own characteristic collision time.

The photons are absorbed following Beer's law, i.e., with a cumulative probability decreasing exponentially with depth. In practice, we proceed as follows: (i) The supercell (simulation box) is first divided in small cubic cells of side $\ell_c=5$ Å. (ii) The instantaneous, *local* absorption coefficient $\alpha_i=\alpha(\mathbf{r}_i,t)$ and (normal incidence) reflectivity $R_i=R(\mathbf{r}_i,t)$ in each cell i (centered at $\mathbf{r}_i$) are then defined as[99]

$$\alpha_i=\alpha_{\mathrm{vc}}(\epsilon_i^*)+\alpha_{\mathrm{fcr}}(\epsilon_i^*)=\frac{2\pi}{n(\epsilon_i^*)\lambda_L}\,\mathrm{Im}\{\epsilon_i^*\} \tag{1}$$

and

$$R_i=\frac{[n(\epsilon_i^*)-1]^2+k^2(\epsilon_i^*)}{[n(\epsilon_i^*)+1]^2+k^2(\epsilon_i^*)}, \tag{2}$$

where the *total* refractive index $n(\epsilon_i^*)$ and extinction coefficient $k(\epsilon_i^*)$ of the excited material are obtained from the instantaneous, *local*, complex permittivity[48]

$$\epsilon_i^*=\epsilon_{\mathrm{vc}}^*(T_i)+\epsilon_{\mathrm{fcr}}^*(N_i). \tag{3}$$

Here, the first term accounts for the single-photon,[100] valence-to-conduction (interband) transitions in the unexcited semiconducting crystal at a temperature[101] $T_i=T(\mathbf{r}_i,t)$ and with band-gap energy $E_{g,i}=E_g(T_i,N_i)\lesssim 1.12$ eV.[102] The second term describes the changes to ϵ_i^* resulting from the free-carrier (intraband) transitions taking place in the Drude electron gas with density $N_i=N(\mathbf{r}_i,t)$.[48,103,104] In the solid, the latter contribution becomes significant at electron densities exceeding the critical plasma density N_{cr} ($\approx 5.9\times 10^{21}$ cm^{-3} in *c*-Si at 266 nm);[48] in the metallic liquid, $\epsilon_{\mathrm{fcr}}^*$ represents the *total* optical response which is assumed to be purely Drudelike.[105,106] (iii) The in-plane x and y coordinates of each photon are subsequently chosen at random; in each case, this determines a column of cells along the z axis which are successively visited starting from the top of the supercell. (iv) In a cell i at an interface separating a gaseous phase from a dense, solid or liquid material—such as the surface of the target or of a cluster in the plume (see below for a definition of the gaseous and dense phases), the photon is reflected (and afterwards ignored) with a probability R_i. However, it is absorbed with a probability $1-\exp(-\alpha_i\ell_c)$ if the material is locally dense: in the crystal, interband and intraband transitions take place with relative probabilities proportional to the ratio of the respective absorption coefficients $\alpha_{\mathrm{vc}}/\alpha_{\mathrm{fcr}}$; in the liquid, photons couple to conduction electrons via intraband transitions (inverse bremsstrahlung). Photoelectric emission is neglected.[107]

As suggested above, this approach relies on the *local* properties of the material; among other benefits, it allows to directly account for the screening of the laser radiation by the plume produced by relatively long, picosecond pulses (see Sec. IV).

Upon interband excitation of one of the (originally four) valence electrons of the atom with position $\mathbf{r}_0$ nearest to $\mathbf{r}_i$, an electron-hole pair is created with total kinetic energy $\hbar\omega_L-E_{g,i}$: each carrier is initially assigned position $\mathbf{r}_0$, velocity $\mathbf{v}_0$ (in a random direction), and kinetic energy $E_k(v_0)=m^*v_0^2/2$, where the effective mass $m^*=0.75m_e$ (the only free parameter in the model) is chosen so as to reproduce the experimental threshold fluence for melting under a laser pulse with $\lambda_L=266$ nm and $\tau_L=15$ ps;[108] in the liquid, an effective mass $m^*=1.75m_e$ is used (m_e is the free-electron mass).[109] In the case of an intraband transition, the energy of the carrier closest to $\mathbf{r}_i$ is increased by an amount $\hbar\omega_L$. Note that carriers may absorb more than one photon during their lifetime.

2. Carrier dynamics

The hot electrons and holes subsequently relax through a cascade of collisional events involving multiple scattering processes.[6,8,27,102] This is simulated using a standard MC approach.[110,111] At every MC (or equivalently MD) time step of duration $\Delta t=1$ fs, a carrier, after traveling a distance $v\Delta t$, has a probability $1-\exp(-\Gamma_0\Delta t)$ of suffering a collision which instantaneously changes its velocity and energy but not its position. Here, $\Gamma_0=1/\tau_0=(1\ \mathrm{fs})^{-1}$ is chosen so that, at all times

$$\Gamma(E_k)=\sum_j \Gamma_j(E_k)=\sum_j 1/\tau_j(E_k)\leqslant \Gamma_0, \tag{4}$$

where the carrier instantaneous (and energy dependent) collisional rate $\Gamma(E_k)$ involves a sum over all physically relevant scattering mechanisms, each characterized by a collision time τ_j. (A fictitious self-scattering mechanism is added to ensure a fixed total scattering rate equal to Γ_0.) Upon the occurrence of a collision, a scattering event j with probability τ_0/τ_j is chosen at random: if appropriate, the carrier kinetic energy is updated and its velocity adjusted accordingly [in both magnitude and (randomly chosen) direction]; in certain circumstances, the carrier may, instead, annihilate (Auger recombination) or new particles may additionally be created (impact ionization). Table I summarizes the various collisional processes and respective scattering times used.

Carrier-carrier scattering allows electrons and holes to exchange energy over a radius of 5 Å. Heating, and eventually local thermal equilibrium at a common electron

TABLE I. Carrier scattering processes and related collision times in solid and liquid silicon; when τ is a function of the carrier energy, references are given instead.

Scattering mechanism	τ (c-Si)	τ (l-Si)
Carrier-carrier[a]	10 fs	10 fs
Carrier-phonon	(see references)[b]	10 fs[c]
Auger recombination	$\geqslant$6 ps[d]	
Impact ionization	(see references)[e]	

[a]References 8 and 27.
[b]M. V. Fischetti and S. E. Laux, Phys. Rev. B **38**, 9721 (1988); M. V. Fischetti, S. E. Laux, and E. Crabbé, J. Appl. Phys. **78**, 1058 (1995).
[c]Typical value for metals [G. L. Eesley, Phys. Rev. B **33**, 2144 (1986)].
[d]E. J. Yoffa, Phys. Rev. B **21**, 2415 (1980); J. Dziewior and W. Schmid, Appl. Phys. Lett. **31**, 346 (1977).
[e]References 112 and 113.

$[T_{e,i}=T_e(\mathbf{r}_i,t)]$ and ion temperature, is achieved through scattering of carriers with (longitudinal-optical) phonons: if $T_{e,i}>T_i$, a quantum of energy of[110] 62.6 meV (c-Si) or 50 meV (l-Si) is given to the nearest atom by adding an appropriate component to its velocity in a random direction.[114] In the crystal, additional collisional processes include Auger recombination and impact ionization: in the former case, the sum of $E_{g,i}$ and the kinetic energy of the recombining electron and hole (near an atom with at least one missing valence electron) is transferred to a neighboring carrier; in the latter case, the energy of the secondary electron and hole generated at $\mathbf{r}_0$ (where $\mathbf{r}_0$ is the position of the impacted atom with at least one valence electron) is computed from the primary carrier energy.[112,113] Thermionic emission is neglected.[115,116]

As pointed out earlier, silicon, like other group IV and III–V semiconductors, is metallic in the liquid state:[105,106,117] upon melting, the average coordination increases from 4 to 6 (and the density from 2.30 to 2.53 g cm^{-3})[118] while the electron density jumps to $\approx 2\times 10^{23}$ cm^{-3}. In our model, the transition from the solid semiconductor to the liquid metal is simulated by locally promoting to the conduction band (with zero initial kinetic energy) the remaining valence electrons of each and every atom which has migrated to the liquid phase; the reverse procedure is carried out upon crystallization. An approach based on a topological analysis of the structure, whereby the diamond elementary building blocks of the silicon crystal are identified, is used to distinguish the periodic solid from the disordered melt.[119] Finally, note that the difference in band-gap energy between the solid and liquid phases acts as a potential barrier which prevents the carriers from diffusing from the latter to the former.

3. Atom dynamics

The motion of the atoms is described using standard MD methodology, excellent accounts of which can be found in the literature.[120] The silicon ions interact via the Stillinger-Weber (SW) potential[121] which exhibits elastic,[122,123] vibrational,[122,124] triple-point,[124,125] and liquid[121,126] properties in good agreement with experiment. It also predicts a first-order transition from a fragile, dense liquid to a strong, low-density and near-tetrahedral, supercooled liquid which could act as a precursor to the ubiquitous solid, amorphous phase in a subsequent glass transition.[127,128] Note, however, that the liquid-liquid transition is observed at a temperature of $\approx$1060 K, i.e., significantly below that at which the "liquid-amorphous" transition is usually assumed to occur ($\approx$1450 K);[129] possible consequences of a lower liquid-to-amorphous transition temperature on the solidification dynamics are discussed in Sec. III A 3.

Note also that the empirical SW potential cannot account for ultrafast, nonthermal phenomena induced in silicon by ultrashort pulses. In the present study, all simulations are carried out well below the threshold for plasma formation ($I_{\text{break}}\sim 10^{13}$ W cm^{-2}) but, in some cases, above that for electronically induced melting ($N\approx N_c$) of a strongly excited covalent solid. However, it should be pointed out that: (i) The "cold" liquid thus obtained is only short-lived and rapidly assumes the usual properties of molten silicon; in this context, it is not likely to influence the ablation and solidification processes taking place on longer time scales. (ii) The observed characteristic time for *thermal* melting under femtosecond irradiation (sufficiently far from the melting threshold) being comparable—albeit slightly longer—to that anticipated for a nonthermal disordering process (see Sec. III A 1), coupling of the laser energy with the irradiated material is not expected to differ significantly in the two cases. Consequently, we expect our simulations to provide a complete, valid picture of the possible thermal routes and related time scales.

4. Simulation setup

Two Si(100) slabs, consisting of 142 560 ($10\times 10\times 30$ nm^3) and 165 600 ($8\times 8\times 50$ nm^3) atoms embedded into a much larger supercell, are used for pulse durations of 500 fs and 100 ps, respectively. Periodic boundary conditions are applied in the x and y directions. In the z direction, normal to the surface, we proceed as follows: (i) To simulate heat diffusion into an infinite bulk, the crystal is terminated by a Langevin heat bath.[120] (ii) To mimic the propagation of pressure waves beyond the bottom of the supercell, a single atomic layer, to which an appropriate set of forces are applied, is added.[71] The originally crystalline substrates are initially equilibrated at $\rho=2.33$ g cm^{-3}, $T=300$ K, and zero pressure.

B. Thermodynamic-analysis method

Insight into the *thermal* pathways to melting, ablation, and solidification under pulsed laser irradiation can be obtained provided the following two conditions are met: (i) The elementary features of the silicon phase diagram are adequately described by the SW potential (see Sec. II B 2). (ii) The structural modifications take place under *local* equilibrium between electrons and ions: apart from the possible nonthermal disordering of covalent semiconducting crystals by ultrashort pulses, recent experiments[13,32,38] confirm that,

below the threshold for plasma formation, absorbing solids evolve thermally on picosecond and longer time scales.

The fulfillment of a local (thermal) equilibrium does not imply, however, that equilibrium between the different—solid, liquid, and gaseous—states of aggregation has been achieved on mesoscopic and macroscopic length scales;[32] in fact, highly transient, nonequilibrium states of matter may develop under femtosecond and picosecond laser irradiation.[13,33,39] In this regard, we show in Secs. III and IV that, by judiciously combining a visual analysis with a thermodynamic description of the irradiated material, metastable states, such as superheated solids or liquids and supercooled melts, can be identified; by further ascertaining where, in the phase diagram, voids begin to develop in the expanding material, we demonstrate that the mechanisms of matter removal can also be determined. This is accomplished using a method first introduced by Perez and Lewis in Ref. 73 and discussed at length in Ref. 74.

1. Computation of local thermodynamic states

As noted above, it is reasonable to assume that most of the system evolution occurs under conditions of local equilibrium between electrons and phonons. In this context, the different routes to changes in long-range order and state of aggregation may be described as a succession of states in ρ-T-P space; this sequence of states will be referred to as the "trajectory" of the system.

In the present study, the density, temperature, and pressure for various sections of the target are obtained at regular intervals in time and the result mapped onto the equilibrium phase diagram of the material (see below). In practice, the target is initially divided (along the z axis) into five-atomic-layer-thick "slices." The following procedure is subsequently carried out at selected points in time: (i) The atoms belonging to the dense (solid or liquid) and gaseous phases—where the latter includes all clusters consisting of 10 atoms or less—are first identified using the Hoshen-Kopelman algorithm;[130] here, the clustering radius is chosen as the mean interatomic distance in a *homogeneous* system with critical-point density $\rho_c = 0.76$ g cm^{-3}, i.e., 3.45 Å. (ii) The supercell is then divided into small cells of side $\ell_c \approx 0.5$ Å, for each of which the closest atom is identified: by summing the volumes of all cells associated with a given atom, an atomic "volume" may, in this way, be defined; in the limit $\ell_c \to 0$, this is equivalent to a tessellation of space into Voronoi polyhedra.[74] (iii) In the specific case of the dense phase, the *surface* atoms, i.e., located in the vicinity of voids, are further distinguished from *volume*, bulk atoms by having at least one cell distant by more than $r_c = 3.77$ Å, where r_c is the SW potential cutoff radius;[121] the latter value ensures that no voids are detected in a *homogeneous* system with density $\rho \leqslant \rho_c$. (iv) A cell belonging to an atom in the gas phase, or distant from an atom in the dense material by more than r_c, is attributed to the gas phase (voids): by later making use of the Hoshen-Kopelman algorithm, the number of internal voids, as well as their respective volumes, can be assessed. (Two cells are assumed to be connected if adjacent to one another.) An example of nucleation of a large cavity in a superheated liquid below the ablation threshold under femtosecond irradiation (see Sec. III C) is depicted in Fig. 2: surface atoms surrounding the void (in green) are shown in red; gas-phase atoms—above the outer surface atoms also in red—are displayed in yellow. (v) The density, temperature, and pressure associated with the condensed and gaseous phases are finally obtained in each slice as detailed in Ref. 74, and the result assigned to dense and gas "branches," respectively; a third, macroscopic branch providing an overall—averaged over the slice—view of the local thermodynamic state of the system is also computed.

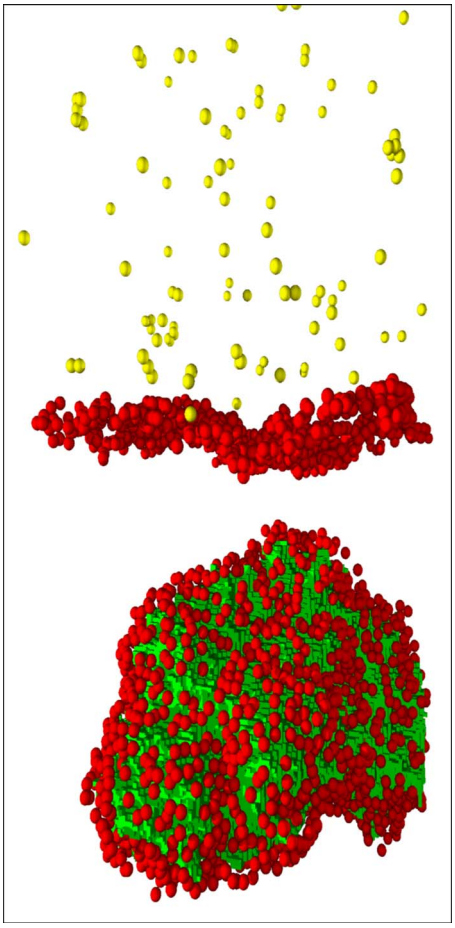

FIG. 2. (Color online) Identification of surface atoms (red), gas-phase atoms (yellow), and internal voids (green); volume atoms are not shown for clarity. See text for details.

In principle, a thermodynamic picture involving the phase diagram is strictly valid for processes taking place at or very near equilibrium. As mentioned earlier, however, transient, metastable states of matter may be identified by combining a visual analysis with the computed local thermodynamic states of the system: e.g., a perfectly ordered crystal above the equilibrium melting temperature T_m and a *homogeneous* liquid below the binodal (see below) indicate superheated solid and liquid states, respectively; similarly, a disordered, liquid structure at a temperature below T_m is associated with nonequilibrium, supercooled states of rapidly cooled matter. In addition, the mechanisms leading to ablation can be inferred by determining where, in the phase diagram, void nucleation—which causes the average and condensed branches to split—takes place.

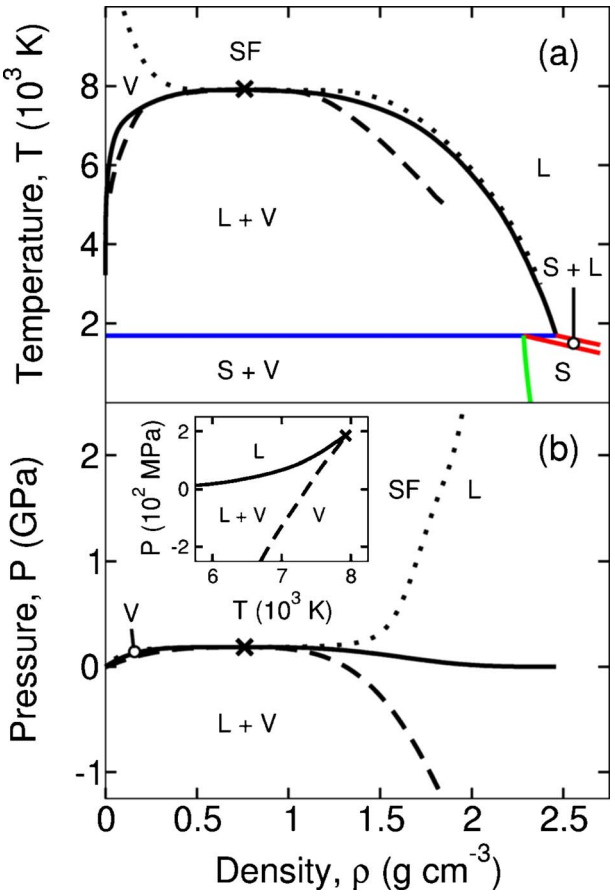

FIG. 3. (Color online) Phase diagram of silicon: (a) ρ-T plane; (b) ρ-P plane; inset: T-P plane. Black solid line: binodal (liquid-vapor coexistence); blue: triple line (solid-liquid-vapor coexistence); green: solid-vapor coexistence line; red: solid-liquid coexistence lines; dotted line: critical isobar and isotherm; dashed line: spinodal; cross: critical point. *S*: solid; *L*: liquid; *V*: vapor; *SF*: supercritical fluid (for $T>T_c$ and $P>P_c$). See text for details.

As shown in Secs. III and IV, this method constitutes a simple, yet powerful, tool for probing the thermodynamic states induced in a solid by laser irradiation.

2. Phase diagram of silicon

The phase diagram of SW silicon is shown in Fig. 3. The binodal has been taken from Refs. 124 and 131. The triple line at the equilibrium melting temperature $T_m=1691$ K (near the experimental value of 1683 K) and the solid-vapor coexistence curve have been obtained from Ref. 124. The solid-liquid coexistence regime is bounded by a low- and a high-density branch (which meet the triple line at 2.28 and 2.45 g cm^{-3}, respectively):[125] while the latter could be deduced from the difference in coordination with the neighboring (sixfold coordinated) liquid region, the former has been approximated by a line parallel to the high-density boundary.[132] The critical isobar and isotherm have been inferred from isochoric-isothermal and isochoric-isobaric MD simulations, respectively. The spinodal and the critical point at $\rho_c=0.76$ g cm^{-3}, $T_c=7925$ K, and $P_c=185$ MPa have been reproduced from Ref. 133.

Note that: (i) A liquid undergoing expansion may transiently penetrate into the metastable region (between the binodal and the spinodal) in a homogeneous state; from a thermodynamic standpoint, large, localized, thermal fluctuations—or, as shown in Sec. III C, the direct conversion of mechanical energy into surface energy—will then favor the widespread, simultaneous nucleation of gas bubbles in the metastable liquid phase, i.e., explosive boiling, on a time scale which varies strongly with the degree of superheating.[13] (ii) In the region below the spinodal, a homogeneous system is mechanically unstable against small perturbations $[(\partial P/\partial\rho)_T>0]$: here, the liquid-to-gas transition is described, rather, by a spinodal decomposition process.[134] (iii) Upon entrance into the liquid-vapor (and solid-vapor) regime, the sound velocity $[c^2=(\partial P/\partial\rho)_S$ where S denotes the entropy] decreases sharply (typically down to a few meters per second);[13,74] as discussed in Sec. III, this is of great significance for the mechanisms of matter removal. (iv) The above phase diagram possesses the essential features which are relevant to a satisfactory qualitative description of group IV and III–V semiconducting materials.[132] In particular, it correctly accounts for the increase in density upon melting (provided heating is carried out at a sufficiently slow rate); this is distinct from the case of, e.g., metals.[77,132] In this view, we expect that the general conclusions drawn in this study also apply to other covalent semiconductors.

III. THERMODYNAMICS UNDER FEMTOSECOND LASER IRRADIATION

The modifications to long-range order and state of aggregation observed in this study for both femtosecond and picosecond pulses are summarized in Fig. 4 and discussed at length in the following sections: (i) Under femtosecond irradiation near the ablation threshold, on the one hand, rapid ($\lesssim 10^{-12}$ s), thermal melting of the excited semiconducting crystal is followed by the expansion of an inhomogeneous, bubble-filled, metallic melt between two well-defined interfaces and the expulsion of a few-nanometer-thick liquid shell, i.e., phase explosion, in a time of $\sim 10^{-12}$–10^{-10} s [Figs. 4(a)–4(e)]; solidification of the nonablated molten material subsequently takes place on a 10^{-11}–10^{-9} s time scale [Fig. 4(f)]. (ii) At higher fluences or longer (picosecond) pulse durations, on the other hand, the ejected matter exhibits, instead, a diffuse, clusterlike structure [Figs. 4(g) and 4(h)]: here, the breakup of the expanding liquid metal follows, rather, from a fragmentation process.

The remainder of this paper is devoted to a thorough analysis of the transient thermodynamic states available to the irradiated material under femtosecond and picosecond pulses. We begin with the thermal routes to melting, ablation, and solidification under ultrashort-pulse laser irradiation.

A. Near-threshold ablation

Figures 4(a)–4(f) portray the various morphological changes taking place during and after irradiation with a 500 fs pulse at the threshold fluence for ablation $F_{\rm th}^{\rm fs}=0.225$ J cm^{-2}. The average irradiance is 5×10^{11} W cm^{-2},

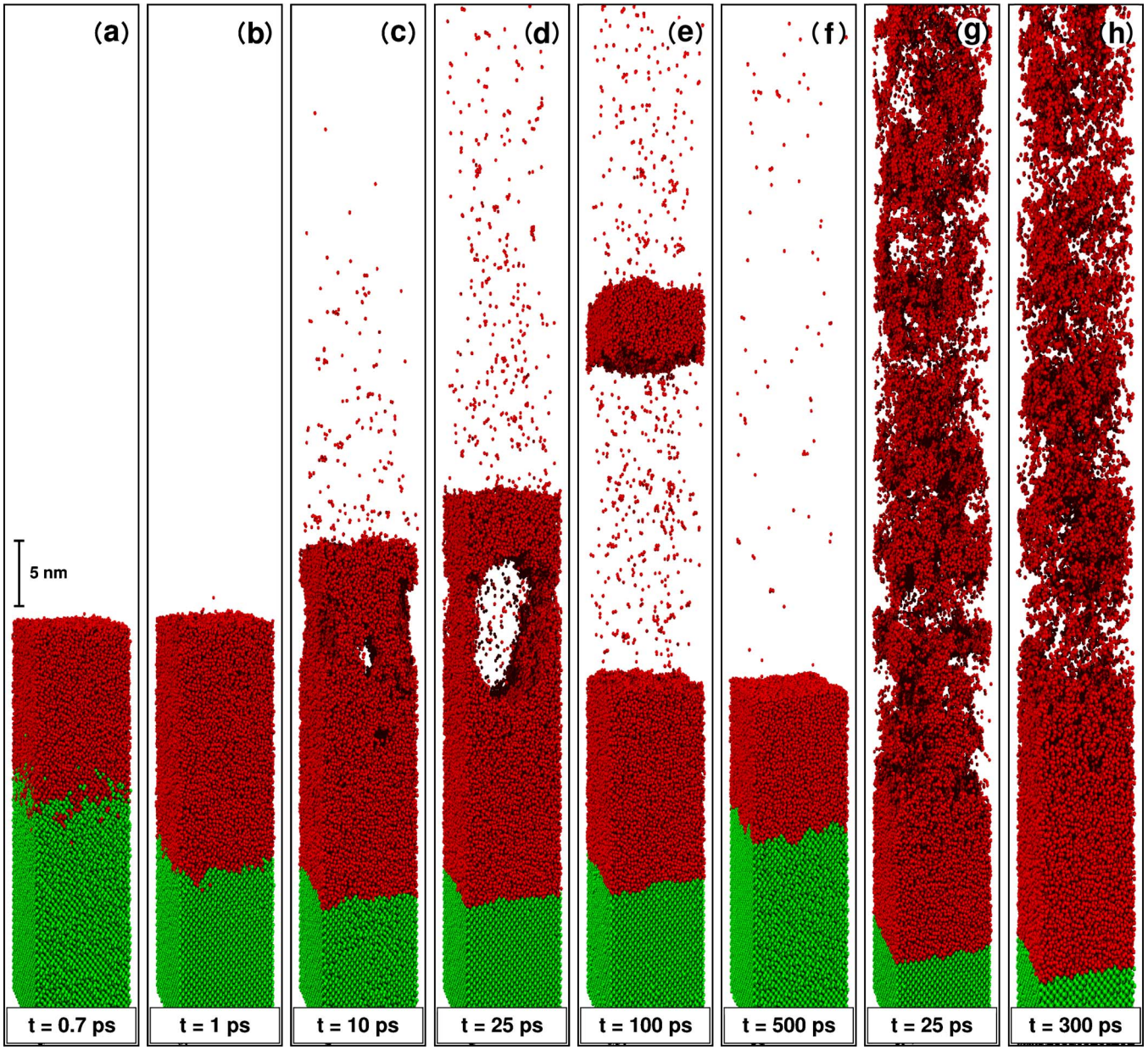

FIG. 4. (Color online) Snapshots revealing the structural changes induced in a Si(100) substrate by 500 fs and 100 ps pulses at 266 nm: (a)–(f) 500 fs pulse at a fluence $F=F_{\mathrm{th}}^{\mathrm{fs}}=0.225$ J cm^{-2}; (g) 500 fs pulse at a fluence $F=2.2F_{\mathrm{th}}^{\mathrm{fs}}=0.50$ J cm^{-2}; (h) 100 ps pulse at a fluence $F=1.1F_{\mathrm{th}}^{\mathrm{ps}}=0.45$ J cm^{-2}; $F_{\mathrm{th}}^{\mathrm{fs}}$ and $F_{\mathrm{th}}^{\mathrm{ps}}$ are the ablation thresholds under femtosecond and picosecond irradiation, respectively. Green: (semiconducting) crystalline silicon; red: (metallic) liquid silicon. Each pulse begins at $t=0$.

i.e., well below I_{break}. The threshold fluence for melting is equal to 0.05 J cm^{-2}.

1. Heating and melting

A typical thermodynamic trajectory for a region of the target originally near the surface is depicted in Fig. 5. The starting point is a crystal at $\rho_0=2.33$ g cm^{-3}, $T=300$ K, and zero pressure (marked *A*). The photons initially generate electron-hole pairs in the unexcited silicon substrate via interband transitions over a penetration depth of $\approx 5-10$ nm; the carrier density eventually increases beyond $N_{\mathrm{cr}}\approx 5.9\times 10^{21}$ cm^{-3} and intraband transitions also occur in the dense, overcritical electron gas. The carriers subsequently reach a common equilibrium state at a temperature $T_e\approx 8000-10\,000$ K through mutual collisions and impact ionization in a time of $\sim 10^{-13}$ s; Auger recombination is not significant on this time scale (see Table I).

The hot electrons and holes simultaneously attempt to equilibrate with the ions by emitting phonons. The heated solid ultimately melts at the surface (as revealed by a visual inspection of the target and the change in local coordination) and the incoming photons thereafter interact primarily with the growing layer of liquid metal via inverse bremsstrahlung [Fig. 4(a)].

The laser energy is converted into lattice vibrational energy in roughly a picosecond.[13] Mechanical expansion is

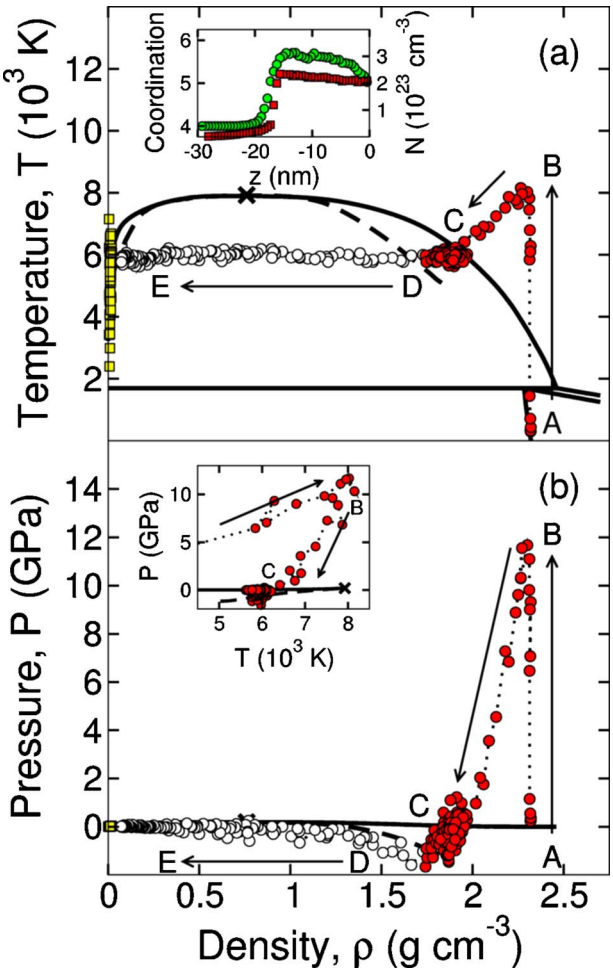

FIG. 5. (Color online) Time evolution of the system in the (a) ρ-T and (b) ρ-P planes for a 500 fs pulse at a fluence $F=F_{\mathrm{th}}^{\mathrm{fs}}=0.225$ J cm^{-2}; the trajectory is for a region of the target initially at a depth of 4 nm below the surface. White circles and dotted line: macroscopic branch; red circles: dense branch; yellow squares: gas branch. Arrows indicate the flow of time. Capital letters refer to locations in the phase diagram (see text). Insets: (a) coordination (green circles) and electron density N (red squares) as a function of distance from the surface z at $t=1$ ps (note the change in properties across the solid-liquid interface at $z\approx-18$ nm); (b) view of the trajectory in the T-P plane.

negligible on this time scale and the system is pulled *away* from the liquid-vapor regime at nearly constant volume ($\rho\approx\rho_0$) to a high-temperature ($T\approx8000$ K) and high-pressure ($P\approx12$ GPa) supercritical state (B): at the end of the pulse, i.e., after a time $t_{\mathrm{liq}}\approx1$ ps, the surface is covered by a hot and highly pressurized liquid layer of thickness $d_{\mathrm{liq}}\approx20$ nm and having metallic properties [see inset in Fig. 5(a)]; below the molten layer lies an intact, semiconducting, bulk crystal at much lower temperature and pressure [Fig. 4(b)].

The following remarks are in order at this point: (i) The system is transiently heated *above* the triple line in a nonequilibrium *crystalline—not* the corresponding *equilibrium* liquid-vapor—state, i.e., the solid becomes superheated; this is further supported by an apparent "melt-front" velocity $d_{\mathrm{liq}}/t_{\mathrm{liq}}\approx2\times10^4$ m s^{-1} well above the (longitudinal) speed of sound $\sqrt{c_{11}/\rho_0}\approx8020$ m s^{-1} (where $c_{11}\approx1.5\times10^{11}$ N m^{-2} is the appropriate elastic stiffness constant of c-Si).[123,135] In this context, melting of the metastable crystal is expected to proceed by homogeneous nucleation of liquid nuclei whose size decreases with superheating $\theta=T/T_m$.[33] In Fig. 4(a), the relatively small liquid inclusions ahead of the "melt front" could indicate a very high degree of superheating or that the material has been heated beyond its limit of mechanical stability at $T_{\mathrm{mec}}\approx2600$ K ($\theta_{\mathrm{mec}}\approx1.54$).[121] Because of the large computational effort involved in the determination of the material thermodynamic trajectory, the same conditions have been simulated in smaller systems but with increased time resolution; results indicate that the solid may be heated to a temperature of ≈3000 K before it starts to melt, thus suggesting a disordering process driven by a mechanical instability in the irradiated crystal; similar conclusions have recently been reported in a MD study of short-pulse laser melting of metal films.[35,36] In contrast, a maximum superheating $\theta\approx1.45<\theta_{\mathrm{mec}}$ is observed under picosecond irradiation (see Sec. IV). (ii) In certain circumstances, the solid may (locally) be superheated without melting (not shown); this is consistent with the experimental observations presented in Ref. 38. (iii) As noted earlier, the empirical SW potential cannot account for the ultrafast, nonthermal melting of silicon at carrier densities in excess of $N_c\approx10^{22}$ cm^{-3};[45] computation of the electron density indicates that the latter value is indeed reached in the present case. Nevertheless, our simulations provide a realistic picture of the possible *thermal* processes and related time scales; in particular, the observed time for thermal melting under femtosecond irradiation, $\sim10^{-12}$ s, agrees well with recent theoretical estimates.[33]

2. Cooling I: expansion and ablation

In order to release the pressure and mechanically equilibrate with the ambient medium, the molten layer subsequently undergoes expansion in vacuum; at the same time, a compressive strain wave (≈5 GPa) is launched from the highly pressurized liquid into the cold, crystalline bulk. A relatively weak tensile pressure wave is also emitted from the latter into the melt; however, the resulting acoustic perturbation is later damped in the expanding liquid-gas mixture characterized by a vanishing sound velocity (see below).[10] In the present context, the strong initial surface pressure gradient leads to the rapid, adiabatic—and consequently isentropic—cooling of the liquid [marked $B\rightarrow C$ in Fig. 5 (see also inset)]: through a conversion of thermal energy into potential and translational energies, the diluting material with flow velocity of ≈500 m s^{-1} enters the liquid-vapor regime (C) where the superheated molten matter is partially transformed into gas on a 10^{-12}–10^{-11} s time scale ($D\rightarrow E$).

Three remarks are in order: (i) From a visual standpoint, the growth of a large, localized cavity in the expanding liquid strongly suggests an explosive-boiling—*not* a spinodal-decomposition—scenario [Figs. 4(c) and 4(d)]. (ii) From a thermodynamic viewpoint, the separation of the dense and macroscopic branches in the metastable region, and the concomitant appearance of a gas branch, confirms a phase-

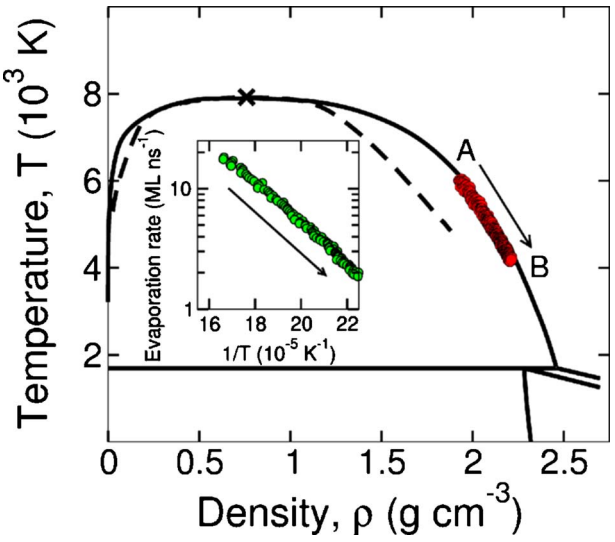

FIG. 6. (Color online) Thermodynamic evolution of the ejected liquid shell in Fig. 4(e). Inset: evaporation rate of the expelled layer as a function of inverse temperature. The density and temperature are averaged over the entire ablated material. Capital letters refer to locations in the phase diagram (see text). See Fig. 5 for the definition of symbols and lines.

explosion process. (iii) Explosive boiling takes place at a temperature of $\approx 0.75T_c$, i.e., significantly below $0.9T_c$. A detailed analysis of the nucleation process in relation with the nature of the ablation threshold will be given in Sec. III C.

The growing cavity eventually percolates through the slab and a few-nanometer-thick liquid shell is removed from the target after a few tens of picoseconds [Fig. 4(e)]. The thermodynamic evolution of the ablated layer on a 10^{-10} s time scale is displayed in Fig. 6: as it moves further away from the surface with a (constant) velocity of ≈ 250 m s^{-1}, the molten material cools by evaporating (marked $A \rightarrow B$); in this regard, the computed evaporation rate (expressed in monolayers per nanosecond) exhibits a clear Arrhenius dependence as a function of inverse temperature (see inset), with a corresponding activation energy of ≈ 3.21 eV. More importantly, the ejected layer (whose thickness is on the order of the optical penetration depth in the initially solid material) evolves *along* the binodal throughout the cooling stage, thus suggesting that a liquid metal achieves equilibrium with its vapor in a time of $\sim 10^{-11}-10^{-10}$ s. As discussed below, this is of great significance for the physical pathways to ablation under picosecond and nanosecond pulses.

Hence, near the threshold fluence for matter removal, our results confirm that an inhomogeneous mixture of liquid and gas expands between two optically flat, reflective interfaces—the ablation front and the boundary separating the nonablated matter from the ejected material; similar conclusions have been obtained in other MD simulations.[14,74] This is also consistent with the observation of optical interference patterns (Newton rings) in time-resolved microscopy experiments on numerous metals and semiconductors.[13]

As the fluence is increased, however, the expanding matter shifts from a subcritical liquid to a supercritical fluid. As will be shown in Sec. III B, this has important consequences for the mechanisms of matter removal.

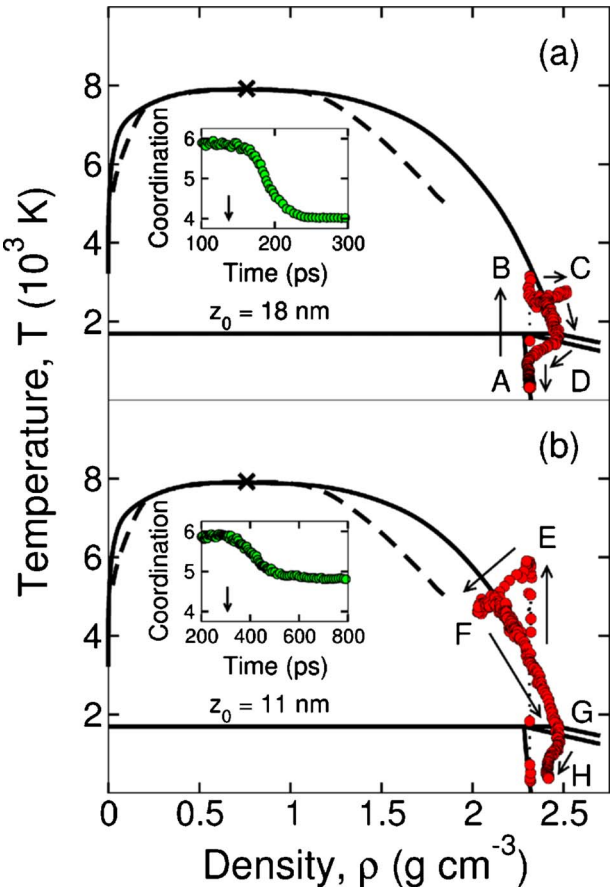

FIG. 7. (Color online) Time evolution of the system in the ρ-T plane for a 500 fs pulse at a fluence $F = F_{\text{th}}^{\text{fs}} = 0.225$ J cm^{-2} and two different depths z_0 below the original surface (as indicated): (a) solidification to a crystalline state; (b) solidification to a glassy state. Insets: local coordination as a function of time (arrows indicate the time at which the equilibrium melting temperature $T_m = 1691$ K is reached upon cooling). Capital letters refer to locations in the phase diagram (see text). See Fig. 5 for the definition of symbols and lines.

3. Cooling II: solidification and final structure

Thermal diffusion into the solid bulk (and evaporation at the outer surface to a lesser extent) is responsible for the cooling and solidification of the nonablated molten material on a $10^{-11}-10^{-10}$ s time scale [Fig. 4(f)]. As shown in Fig. 7, two distinct physical pathways are observed: (i) Deep into the metallic liquid layer [Fig. 7(a)], the neighboring crystalline phase acts as a seed for *heterogeneous* crystallization from the melt (marked $A \rightarrow B \rightarrow C \rightarrow D$); the transition from a disordered liquid with average coordination of ≈ 6 to a fourfold coordinated, ordered structure confirms this (see inset). (ii) Closer to the surface [Fig. 7(b)], the material is initially heated to a higher temperature (E); the resulting liquid subsequently expands toward the binodal ($E \rightarrow F$). As a result of insufficient translational energy (see Sec. III C), homogeneous nucleation of gas does not take place in the super-

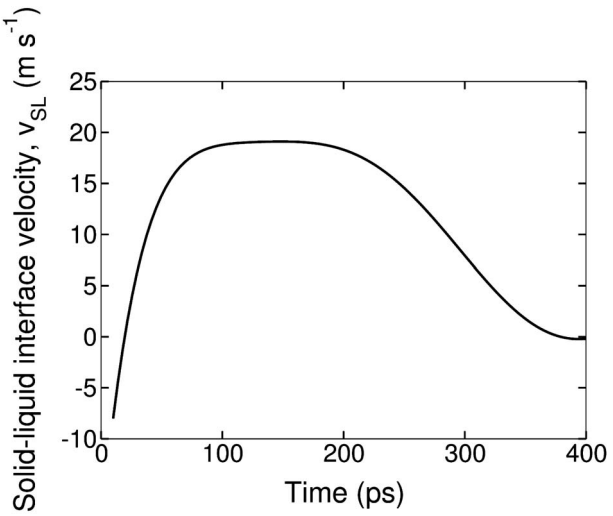

FIG. 8. Velocity of the interface between the solid (crystal) and liquid phases as a function of time following irradiation with a 500 fs pulse at a fluence $F=F_{th}^{fs}=0.225$ J cm^{-2}; negative and positive values indicate melting and solidification (crystallization), respectively.

heated melt (F) and the system is later slowly cooled under liquid-vapor coexistence ($F\rightarrow G$). The triple line is eventually crossed and the liquid becomes *supercooled* (G); visual inspection of the nonablated material confirms that (locally) the (equilibrium) solid-liquid and solid regions of the phase diagram are accessed in a disordered, metastable state. However, crystallization does not occur for the following reasons: (a) The system standing relatively far from the solid-liquid interface, a heterogeneous liquid-to-crystal transition is not possible. (b) The energy required to *homogeneously* nucleate critical nuclei of the stable crystalline phase into the supercooled melt decreases with temperature, i.e., with increased supercooling; however, this also translates into a significant decrease of the atomic mobility and a corresponding increase of the liquid-to-crystal relaxation time. Consequently, the structure, several hundred degrees below T_m, is ultimately "frozen" into an intermediate state with coordination between that of the liquid and the crystal (see inset): the molten material transforms into a *glass* (at $\approx$900 K) which subsequently cools to 300 K (H).

Figure 8 displays the solid-liquid interface velocity v_{SL} as a function of time. As can be seen, the solidification process begins after a few tens of picoseconds and is complete after a few hundreds of picoseconds, in good agreement with experimental data;[30] the observed regrowth velocity of $\approx$10–20 m s^{-1} also compares favorably with experiment[11,12] and other MD studies.[136]

Three distinct stages can be identified: (i) Efficient heat conduction into the solid initially gives rise to an increase of the regrowth velocity ($t\lesssim$100 ps). (ii) This takes place until heat flow is balanced out by the rate of latent heat release (which increases as more liquid is converted into a crystal), at which point a steady-state regime is achieved at $v_{SL}=18$ m s^{-1} ($100\lesssim t\lesssim 200$ ps). (iii) As noted above, however, the atomic mobility decreases and the liquid-to-crystal relaxation time eventually increases as the supercooled molten material further cools ($t\gtrsim$200 ps): v_{SL} decreases and crystallization of the melt stops on a 10^{-10} s time scale; as a result, a layer of "frozen," uncrystallized liquid with thickness of $\approx$10 nm is left at the surface [Fig. 4(f)].

Note that a transition from a disordered liquid to a near-fourfold-coordinated, short-range-ordered *amorphous* phase above a threshold regrowth velocity of $\approx$15 m s^{-1} has been discussed in several experimental investigations of laser-induced melting and solidification of silicon.[11,12,40,137,138] However, such a transition is not seen in the present study; similar conclusions have also been reported in other MD simulations involving the SW potential.[136] Two reasons could explain the observed discrepancy: (i) From a thermodynamic standpoint, the predicted liquid-to-amorphous temperature (slightly under 1060 K), below which the melt needs to be supercooled for the transition to take place, is significantly lower than the experimentally derived value of $\approx$1450 K.[129] (ii) From a kinetic viewpoint, a possible explanation could be a higher threshold regrowth velocity in SW silicon.[139]

B. Ablation at higher fluences

As suggested by Fig. 4(g), far-from-threshold femtosecond irradiation involves different pathways to ablation. In this respect, two observations can be drawn from a comparison with Figs. 4(d) and 4(e): (i) The removal of molten material does *not* take place by the growth of a highly localized cavity between two sharp interfaces and the subsequent ejection of a liquid shell; instead, the expanding plume displays a diffuse, clusterlike structure without a well-defined ablation front. (ii) The ejected liquid expands noticeably faster. As shown below, such differences are associated with expansion in a different region of the phase diagram.

Figure 9 illustrates the transition to a new regime. The scenario is as follows: (i) Similarly to near-threshold irradiation, the system is pulled *away* from the region of metastable states upon near-isochoric heating of the material; in Fig. 9(a), which is for the maximum average irradiance of 1×10^{12} W cm^{-2} investigated in this work, the result is a hot ($T\approx$16 000 K), highly pressurized ($P\approx$28 GPa) supercritical fluid at near-solid density (marked A). (ii) The liquid-vapor regime is subsequently approached upon rapid, adiabatic cooling of the expanding matter with maximum flow velocity of $\approx$800 m s^{-1} ($A\rightarrow B$); a strong ($\approx$14 GPa) compressive strain wave is also emitted from the molten layer into the solid bulk. (iii) However, the binodal is *not* reached in a homogeneous state: instead, the split of the dense and macroscopic branches, which indicates the onset of ablation, takes place in the supercritical regime, i.e., *outside* of any phase coexistence region (B); the same conclusions emerge from inspection of the trajectory in the ρ-P plane (see inset). In regions standing further from the surface, the molten material, following a short incursion into the metastable region, is cooled along the binodal and matter removal is not observed (C).

Undoubtedly, ablation cannot be attributed, in the present case, to a phase transition such as, e.g., explosive boiling or spinodal decomposition; vaporization is also excluded since

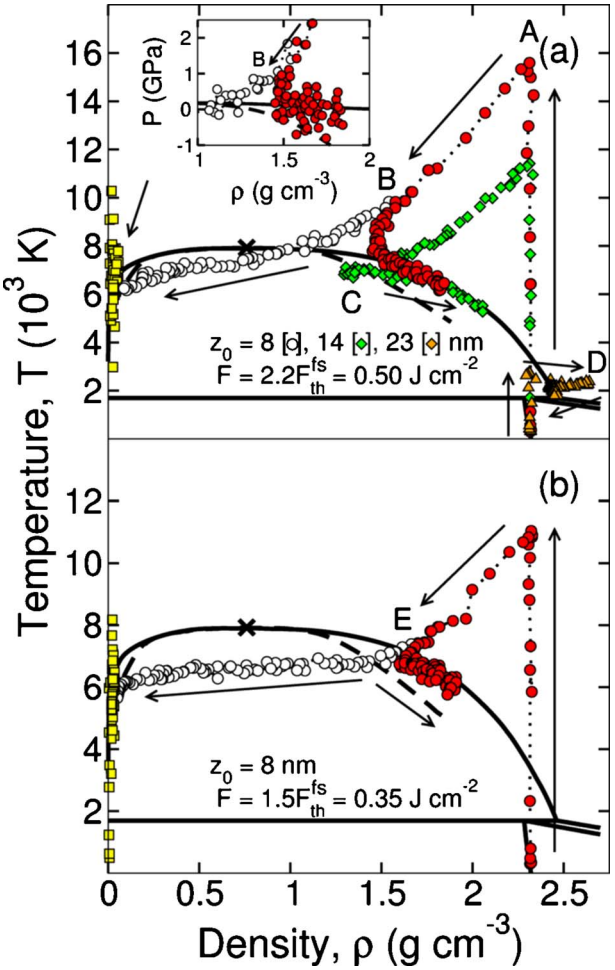

FIG. 9. (Color online) Time evolution of the system in the ρ-T plane for a 500 fs pulse at two different fluences F and various depths z_0 below the original surface (as indicated). Inset: zoom on the trajectory for z_0=8 nm in the ρ-P plane. White circles and dotted line: macroscopic branch; red circles: dense branch; yellow squares: gas branch; green diamonds and orange triangles: additional macroscopic branches. Arrows indicate the flow of time. Capital letters refer to locations in the phase diagram (see text).

fairly large clusters are produced in the dissociation process.

The above picture is analogous to that recently reported in a MD study of femtosecond irradiation and ablation of a two-dimensional Lennard-Jones system.[73,74] At fluences relatively far from the threshold for matter removal, the rapid expansion is such that the equilibrium structure of the *supercritical* material can no longer be preserved by atomic diffusion: the expanding matter undergoes a *nonequilibrium* transition from a homogeneous fluid to a heterogeneous, clustered phase through a "nontrivial" *fragmentation* process; in this case, the average fragment size depends upon the local strain rate, i.e., the translational velocity *gradient* normal to the surface. Note that: (i) This phenomenon is qualitatively different from spallation or cavitation whereby the breakup of the material is assisted by tensile strain waves. (ii) As discussed in Sec. IV, matter removal under picosecond pulses is also driven by a fragmentation process; however, the latter takes place *near thermodynamic equilibrium* and is said, instead, to be "trivial."[74,77]

The differences in expansion dynamics between near- and far-from-threshold femtosecond irradiation are best understood within a one-dimensional self-similar rarefaction-wave (SSRW) model;[13,15,54,74] the latter describes the propagation of the rarefaction (density decrease) wave into the bulk molten material as the heated liquid layer expands in vacuum. In principle, the SSRW model is strictly valid for an instantaneously and homogeneously heated solid at uniform density ρ_i; however, we show below that it is also suitable for a qualitative understanding of the ablation process taking place in the present "real" conditions.

According to this model, the increase in translational (flow) velocity du, for an infinitesimal increase in density dρ, is proportional to the sound velocity $c(\rho)$; the translational velocity at density ρ_f reads

$$u_f(\rho_f,S) = -\int_{\rho_i}^{\rho_f} \left(\frac{c(\rho)}{\rho}\right)_S d\rho, \tag{5}$$

where S denotes the entropy (a "minus" sign is added to ensure that expansion in vacuum is described by *positive* velocities). The strong dependence of the speed of sound on density is of great significance here: as detailed in Refs. 37 and 74, the sharp drop of $c(\rho)$ in the liquid-vapor coexistence regime implies a subcritical, metastable material with flow velocity u_f nearly *independent* on ρ_f and S; upon supercritical expansion, however, the drastic decrease of the sound velocity is not observed and the expanding fluid is expected to be characterized by significantly higher, density- and entropy-dependent translational velocities.

This has the following consequences: (i) Near the ablation threshold, the system enters the metastable region upon cooling and the various sections of the superheated material (which follow different subcritical isentropes) possess similar translational velocities; as depicted in Fig. 4(d), this leads to a heterogeneous mixture of liquid and gas with a steplike density profile—the sharp ablation front—giving rise to the optical interference patterns observed in time-resolved microscopy experiments.[13] (ii) At higher fluences, however, the flow-velocity *gradient* across the supercritical diluting fluid is significantly higher. In this case, it is expected that (a) the density drops smoothly across the ablating material which, consequently, does not exhibit a steep liquid-vacuum boundary and that (b) the breakup of the rapidly expanding matter results from a ("nontrivial") fragmentation process. Both a visual inspection of the system in Fig. 4(g) and the disappearance of the Newton rings at relatively high fluences (but before the onset of plasma formation) support the above conclusions;[38,74,98] in particular, the transition between the phase-explosion and fragmentation regimes in silicon [marked E in Fig. 9(b) where the split of the dense and macroscopic branches takes place at the liquid-vapor boundary and at near-critical temperature] occurs at a predicted fluence of $\approx 1.5F_{th}^{fs}$ which agrees remarkably well with experiment.[98]

Metals—which *expand* upon melting and whose thermodynamic properties can be *qualitatively* described by, e.g., the Lennard-Jones phase diagram in Ref. 74—and semiconductors exhibit different solid-liquid features.[77,132] This

translates into the following differences under femtosecond irradiation: (i) Unlike semiconducting materials, metals, for which the initial state does *not* lie below the triple line, can remain *solid* at temperatures significantly above T_c;[74] as a result, melting can also be observed upon *cooling* to the solid-liquid (or liquid) region. (ii) In a very narrow range of fluences near the ablation threshold, the *cooling* metallic system can be pulled by tensile strain waves toward the *solid*-vapor coexistence regime where the breakup of the mechanically unstable *solid* material is described by a spallation process;[74] this is unlikely to take place in semiconductors such as silicon where melting occurs at relatively low temperatures ($T \ll T_c$) upon *heating*, and where ablation therefore involves the ejection of *liquid* matter upon rapid cooling to the *liquid*-vapor regime. (iii) As a result of a liquid phase with higher density than the solid in group IV and III–V covalent materials, melting of the superheated crystal can be assisted by a *compressive* strain wave emitted from the upper, highly pressurized liquid layer [marked *D* in Fig. 9(a)].

However, in view of phase diagrams with similar liquid-vapor and supercritical features,[77,132] metals and semiconductors display common thermal routes to matter removal under near- and far-from-threshold femtosecond irradiation; as noted earlier, this is confirmed by both experiment[13,38] and numerous MD studies.[14,73,74,76,77] In Sec. IV, we present results which strongly suggest that this universal behavior may be extended to longer, picosecond (and possibly nanosecond) pulses.

C. Nature of the ablation threshold

Evidence for a well-defined threshold fluence—below which matter removal is driven by evaporation and above which large, macroscopic amounts of material are ejected from the irradiated surface—has been reported under femtosecond,[13,38,91] picosecond,[62] and nanosecond[64–66] irradiation of metals and semiconductors. This has also been observed in several MD investigations of laser ablation;[36,71,74,76,80,140,141] in the present study, an increase of the fluence by only a few percent (under both femtosecond and picosecond pulses) is sufficient to cause sudden, massive ejection of molten material.

In spite of its ubiquitous nature, the origin of the threshold behavior has, to date, remained unclear. In general, it is postulated that the onset of ablation results from the strong increase with temperature of the bubble nucleation rate in a strongly superheated melt:[13,96,142] i.e., near-threshold matter removal is described as a nonequilibrium process driven by large, localized, *thermal* fluctuations in a metastable liquid. In Ref. 96, in particular, the relatively high flow velocities characterizing the expanding material upon entrance into the liquid-vapor regime have not been taken into account.

At fluences near the ablation threshold, we find that the initial increase in translational energy of the expanding molten matter is followed by a rapid decrease of the flow velocity and the *concomitant* growth of a large cavity within the diluting material; this suggests that the rapid expansion of the liquid may play a role in the bubble nucleation process.

In the following discussion, we give strong evidence that the threshold behavior is, to a significant extent, *mechanical* in nature; more specifically, it is shown that bubble nucleation in the metastable liquid is initiated by the conversion of *translational* energy into surface energy, *not* by highly localized thermal fluctuations. Note that the analysis given below applies only to covalent semiconductors under femtosecond irradiation where near-threshold ablation is governed by explosive boiling; it does not describe the case of metallic systems[74,140] and organic solids[71] where the threshold dynamics are likely to be determined, rather, by spallation.[143]

Figure 10 portrays the bubble nucleation process near, but *below*, the threshold fluence for matter removal; the corresponding thermodynamic trajectory is displayed in Fig. 11. In addition, Fig. 12 provides information on the time dependence of various quantities of interest in the initially expanding and subsequently contracting molten layer: (i) The total volume occupied by cavities V_c and their total number in the liquid (as obtained following the method presented in Sec. II B 1) are first shown in Fig. 12(a). (ii) The molten layer is divided into thin (≈ 5 Å) slices at various points in time. In each slice containing N_a atoms of equal mass m, we proceed as follows: (a) The center-of-mass velocity v_{cm} (in the z direction) is computed and the local *translational* energy defined as $N_a m v_{\mathrm{cm}}^2/2$. (b) The N_s surface atoms in the vicinity of internal voids, but *not* at the outer surface, and N_v volume atoms in the bulk material are identified as described in Sec. II B 1; the local *surface* energy is then defined as $N_s(E_s - E_v)$, where E_s and E_v are the average potential energies of the surface and volume atoms, respectively. The liquid *total* translational and surface energies in Fig. 12(b) are finally obtained by summing over all slices. (We have verified that, within a satisfactory range, the result does not depend on the thickness of the slices.)

The evolution of the system under *subthreshold* femtosecond irradiation can be divided into five successive stages:

(i) The laser energy is first converted into heat in about a picosecond, which is too short for significant expansion to occur; here, the resulting state corresponds to a *subcritical* liquid at $\rho \approx 2.33$ g cm^{-3}, $T \approx 7200$ K, and $P \approx 10$ GPa (marked *A* in Fig. 11).

(ii) The liquid-vapor regime is then approached upon rapid, adiabatic cooling ($A \rightarrow B$): the molten layer expands and its translational energy increases until the metastable region is reached at $t \approx 3$ ps (B). The consequences of the subsequent abrupt drop of the sound velocity are twofold: (a) The flow velocity stops increasing [see Eq. (5)]; as a result, the translational energy reaches its maximum value [Fig. 12(b)]. (b) The superheated material is thereafter characterized by a well-defined liquid-vacuum boundary; as can also be appreciated from Fig. 10(a), the metastable liquid is still rather homogeneous at this point.

(iii) In the following few picoseconds ($3 \lesssim t \lesssim 5$ ps), the *translational* energy gained upon cooling is rapidly converted into *surface* energy and expansion slows down. This can be seen from the steep rise in the number of independent cavities in Fig. 12(a); visual inspection of the system confirms that small, subnanometer-sized voids have been created in the metastable liquid [Fig. 10(b)]. Note also that the total decrease in translational energy agrees closely (in absolute

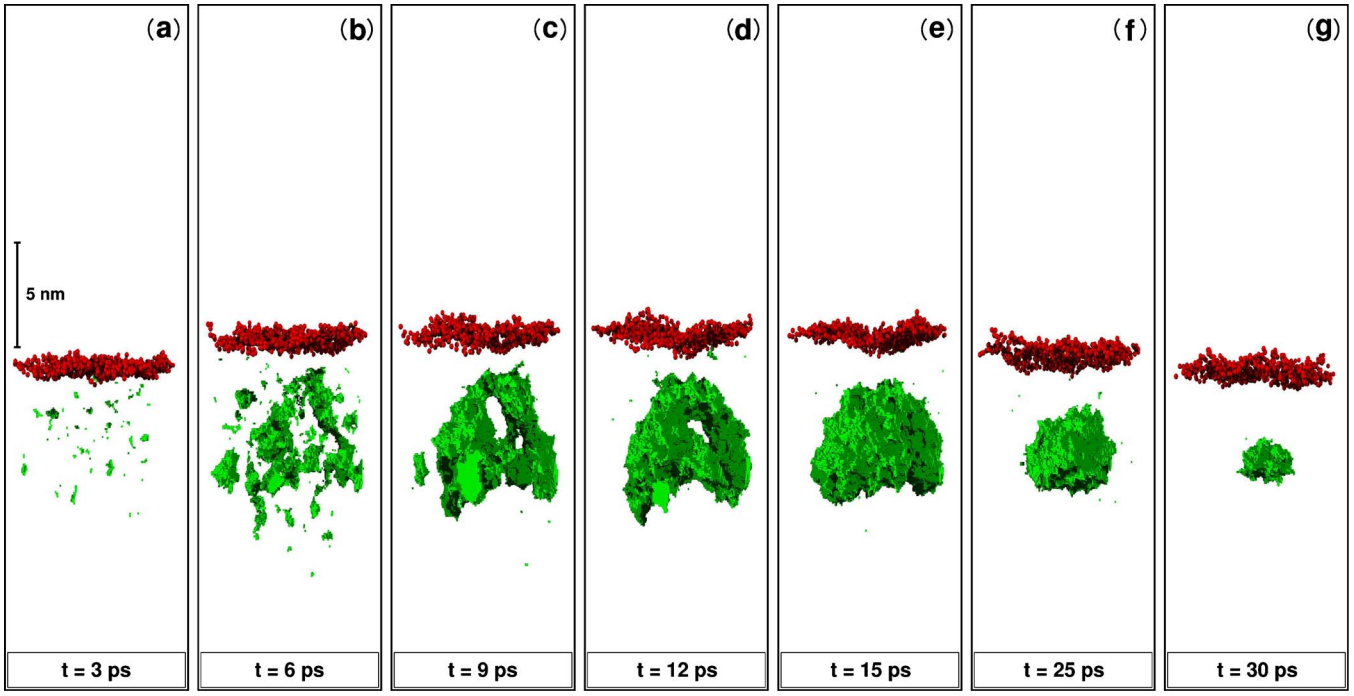

FIG. 10. (Color online) Snapshots illustrating the growth and subsequent collapse of a cavity (green) below the surface (red) following irradiation with a 500 fs pulse at a (subthreshold) fluence $F=0.9F_{\mathrm{th}}^{\mathrm{fs}}=0.20$ J cm^{-2}; gas-phase atoms are not shown. The pulse begins at $t=0$.

value) with the *simultaneous* total increase in surface energy [Fig. 12(b)].

(iv) At later times ($5 \lesssim t \lesssim 15$ ps), during which the total *surface*, but not the volume, is conserved, the further expansion of the liquid is driven by the growth of a cavity below the surface. This occurs in two distinct steps: (a) As can be seen from the decrease in the number of cavities in Fig. 12(a) and a comparison of Figs. 10(b) and 10(c), void coalescence first takes place in the superheated liquid ($5 \lesssim t \lesssim 10$ ps). (b) The resulting large cavity later grows to reach a maximum volume of ≈ 135 nm^3 at $t \approx 15$ ps and expansion of the molten layer stops [Figs. 10(d), 10(e), and 12(a)]; this can also be inferred from the split of the dense and macroscopic branches in Fig. 11 ($B \rightarrow C$). Note that the total surface energy remains *constant* during coalescence and growth [Fig. 12(b)]: it is easy to show that, for equal surfaces, the total volume occupied by two (or more) voids is smaller than that occupied by a single cavity; in other words, bubble nucleation in the superheated melt can be seen as a rapid rearrangement of the total surface initially created by conversion of translational energy into surface energy.

(v) As a result of insufficient translational energy to grow a critically-sized nucleus of the stable vapor phase into the metastable liquid phase, the cavity subsequently collapses [Figs. 10(f) and 10(g)]; this is also apparent from the corresponding decrease of V_c [Fig. 12(a)]. The temperature increase in Fig. 11 ($C \rightarrow D \rightarrow E$) and simultaneous decrease of the total surface energy in Fig. 12(b) indicate that the latter is dissipated into heat. The material is then cooled by thermal conduction along the binodal and eventually solidifies (to a glass in this case) on a 10^{-10} s time scale ($E \rightarrow F$).

The following remarks are in order: (i) As mentioned earlier, the threshold behavior governing the onset of explosive boiling in covalent semiconductors is, to a significant extent, *mechanical* in nature: here, the relatively high translational energy gained upon cooling to the liquid-vapor regime—*not* large, localized, thermal fluctuations—provides the energy required to grow critically-sized nuclei of gas in the superheated liquid; the remaining translational energy is carried away by the ejected liquid shell moving with constant velocity. (ii) As a result of the rather small lateral dimensions of the system in the present study, the threshold behavior is

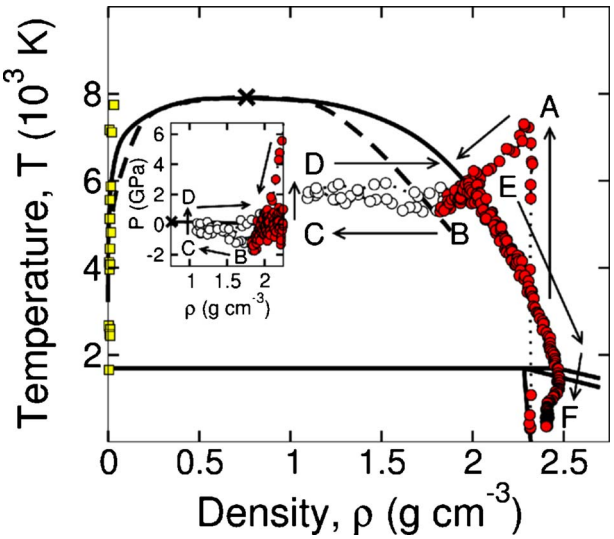

FIG. 11. (Color online) Typical thermodynamic trajectory for the region where nucleation of the large cavity takes place in Figs. 10(a)–10(g). Inset: view of the trajectory in the ρ-P plane. Capital letters refer to locations in the phase diagram (see text). See Fig. 5 for the definition of symbols and lines.

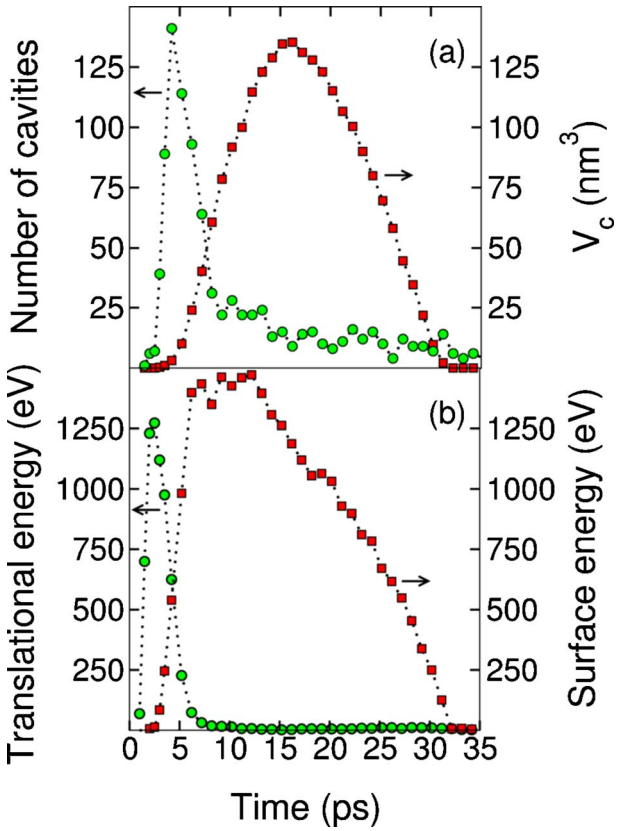

FIG. 12. (Color online) Time dependence of various quantities characterizing the molten layer produced upon irradiation with a 500 fs pulse at a (subthreshold) fluence $F=0.9F_{\mathrm{th}}^{\mathrm{fs}}=0.20$ J cm^{-2}: (a) total number of cavities (green circles) and total volume occupied by cavities V_c (red squares) in the liquid; (b) total translational (green circles) and surface (red squares) energies of the liquid.

determined, instead, by the minimum translational energy needed to grow a nucleus that will percolate through the slab; it is therefore likely that the "true" threshold fluence for matter removal is somewhat underestimated. (iii) In Ref. 13, the flow velocity at the liquid-vacuum boundary is approximated as $u_\ell \approx c_0 \ln(\rho_0/\rho_b)$ [see Eq. (5)], where ρ_0 and ρ_b are the solid density and liquid density at the binodal (marked E in Fig. 11), respectively; c_0 is the sound velocity of the unperturbed material. In view of the above discussion, however, it is clear that u_ℓ ($\approx$1000 m s^{-1} at the threshold fluence) significantly overestimates the velocity of the layer ejected upon near-threshold femtosecond irradiation [$\approx$250 m s^{-1} in Fig. 4(e)].

IV. THERMODYNAMICS UNDER PICOSECOND LASER IRRADIATION

The thermodynamic pathways observed under femtosecond laser irradiation have revealed phase-change phenomena driven by metastable states of rapidly heated or promptly cooled matter: upon thermal melting (see note concerning possible nonthermal effects in Sec. III A 1), on the one hand, the transient, superheated solid presumably crosses the limit of mechanical stability before disordering to a metallic melt; upon solidification, on the other hand, long-lived, supercooled liquid states are involved in a direct liquid-to-glass transition.

In the vicinity of the threshold fluence for matter removal, the phase-explosion-like transition from a homogeneous, aggregated, and disordered state to a heterogeneous mixture of liquid and gas is associated with short-lived, metastable states of matter: the molten material is *cooled* to the two-phase regime before liquid-vapor equilibrium is achieved and, consequently, becomes *superheated*. At higher fluences, however, ablation does not result from a phase transition and high strain rates, not highly superheated states, are responsible for the nonequilibrium fragmentation process.

In all phase transitions observed under femtosecond irradiation, equilibrium is locally achieved between electrons and ions, but *not* among the different—solid, liquid, and vapor—states of aggregation on larger—mesoscopic—length scales. Hence, phase change can be regarded as a *nonequilibrium* thermal process involving transient, superheated or supercooled, thermodynamic states.

As noted in Sec. III, the material ejected under picosecond pulses exhibits a diffuse, clusterlike structure very different from that observed under near-threshold femtosecond irradiation but, however, remarkably similar to that obtained following (nonequilibrium) fragmentation of an expanding fluid with ultrashort pulses at higher fluences [see Figs. 4(d), 4(g), and 4(h)]. We show below that matter removal under picosecond irradiation can also be described by a fragmentation process; in particular, significantly slower expansion allows liquid-vapor equilibrium to take place, and explosive boiling to be suppressed, on a $\sim 10^{-11}-10^{-10}$ s time scale.

A. Dynamics under subcritical expansion

Figure 13 displays the various morphological changes taking place during and after irradiation with a 100 ps pulse slightly above the threshold fluence for matter removal $F_{\mathrm{th}}^{\mathrm{ps}}=0.40$ J cm^{-2}; the average irradiance is equal to 5×10^9 W cm^{-2}. The corresponding thermodynamic trajectories are depicted in Fig. 14.

A typical pathway under *subcritical* expansion is shown in Fig. 14(a); the associated initial depth corresponds to a section of the *nonablated* matter slightly below the boundary separating the ablating, volatile plume from the subthreshold material. The laser pulse originally gives rise to interband transitions in the initially unexcited solid at $\rho=2.33$ g cm^{-3} and $T=300$ K (marked A). Upon absorption of additional photons in the crystal, more electron-hole pairs are created and the carrier density increases to reach a maximum value of $\approx 3\times 10^{21}$ cm^{-3} after a few tens of picoseconds.[144] In the present case, intraband absorption is negligible in the undercritical electron gas ($N<N_{\mathrm{cr}}$); however, carrier diffusion, impact ionization, and Auger recombination are all significant on a $10^{-11}-10^{-10}$ s time scale.

The deposited energy is simultaneously transferred to the ions through scattering of the carriers with phonons. The solid is rapidly heated ($\sim 10^{13}$ K s^{-1}) and a maximum superheating $\theta\approx 1.45$ ($T\approx 2450$ K) is achieved in the perfectly ordered, metastable crystal (B). This corresponds to a tem-

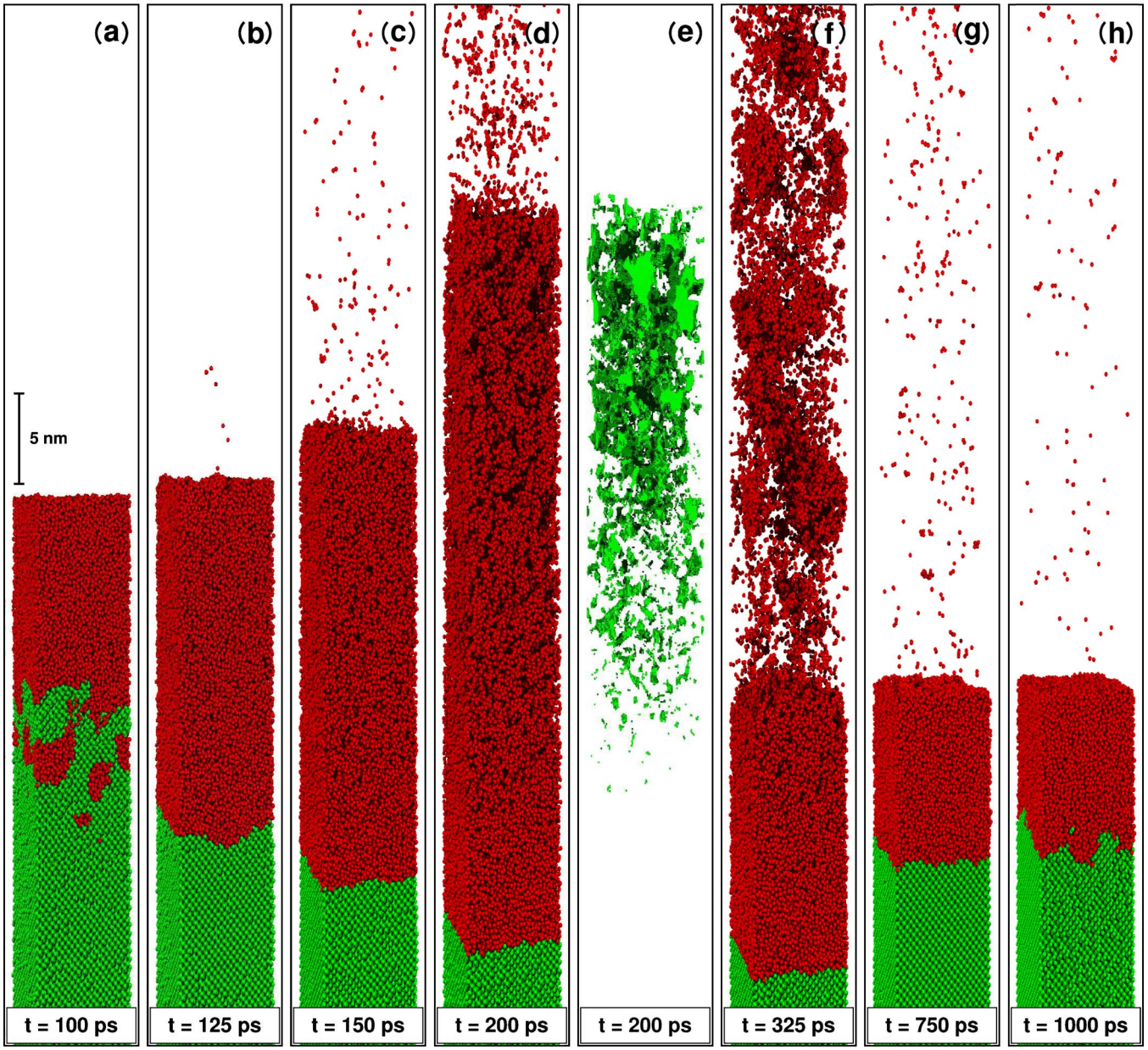

FIG. 13. (Color online) Snapshots revealing the structural changes induced in a Si(100) substrate by a 266 nm, 100 ps pulse at a fluence $F=1.1F_{\mathrm{th}}^{\mathrm{ps}}=0.45$ J cm^{-2}: (a)–(d) and (f)–(h) green: (semiconducting) crystalline silicon; red: (metallic) liquid silicon; (e) view of the voids in the expanding molten layer. The pulse begins at $t=0$.

perature ≈750 K above T_m but, nevertheless, *below* the limit of mechanical stability at ≈2600 K (see Sec. III A 1); reports of semiconducting materials superheated by several hundred degrees above their equilibrium melting temperature under picosecond pulses can be found in, e.g., Refs. 11, 29, and 30.

The metastable crystalline state is only short-lived and *homogeneous* nucleation of liquid nuclei in the strongly heated solid takes place in a time of $\sim 10^{-12}$–10^{-11} s [Fig. 13(a)]: these grow ahead of the apparent "melt front" characterized by a maximum velocity of $\sim 10^3$ m s^{-1}; at later times—upon slower heating and reduced superheating—the solid-liquid interface propagates *heterogeneously* into the bulk crystal with a velocity of $\sim 10^2$ m s^{-1} [Figs. 13(b)–13(d)].[145] Note that competing heterogeneous and homogeneous melting mechanisms have also been reported in a recent MD study of short-pulse laser irradiation of metallic films.[36]

The irradiated solid *cools* (due to the consumption of latent heat) and densifies to a sixfold-coordinated structure upon disordering to a liquid ($B \rightarrow C$); the resulting molten material is momentarily at a *lower* temperature than the superheated bulk crystal, and the corresponding *negative*[146] ($\partial T/\partial z < 0$) temperature gradient gives rise to a temporary reversal of the direction of heat flow at the surface [see inset in Fig. 14(a)].[147] The liquid subsequently couples with the incoming photons through inverse bremsstrahlung and heating of the metallic melt takes place ($C \rightarrow D$). The system

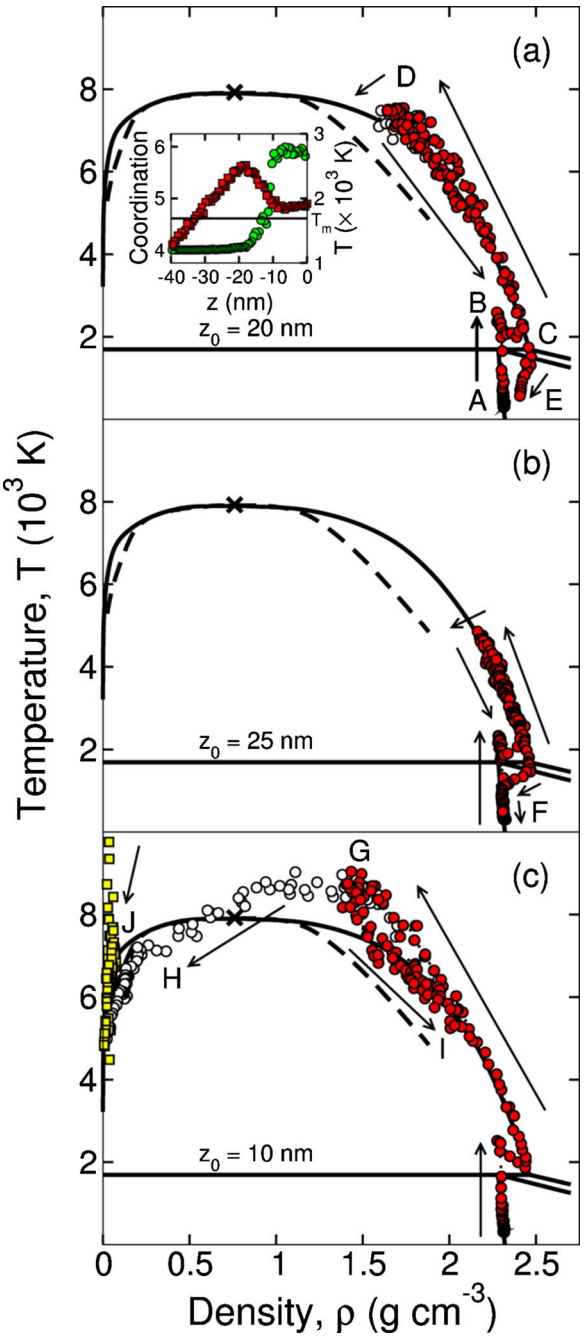

FIG. 14. (Color online) Time evolution of the system in the ρ-T plane for a 266 nm, 100 ps pulse at a fluence $F=1.1F_{\mathrm{th}}^{\mathrm{ps}}=0.45$ J cm^{-2} and various depths z_0 below the original surface (as indicated). Inset: coordination (green circles) and temperature T (red squares) as a function of distance from the surface z shortly after the onset of melting; the solid-liquid interface is at $z\approx-12$ nm; the equilibrium melting temperature T_m is marked by the horizontal line. Capital letters refer to locations in the phase diagram (see text). See Fig. 5 for the definition of symbols and lines.

(locally) is eventually left (at the end of the pulse) in a *subcritical* state at near-critical temperature $T\approx0.95T_c$ ($\approx$7500 K) and pressure $P\approx1.35P_c$ ($\approx$250 MPa), and with *nearly zero flow velocity* (D).

Two differences readily emerge from a comparison with near-threshold femtosecond irradiation [Figs. 4(a)–4(f) and 5]: (i) In light of the much longer pulse duration, significant expansion and surface evaporation occur during the slower heating of the melt [Figs. 13(a)–13(d) and 14(a)]; in the present case, about 3% of the incident laser radiation is screened by the plume (see Sec. II A 1). (ii) More importantly, the subsequently cooling liquid, at a relatively low pressure, expands very slowly. This has the following two consequences: (a) The penetration into the liquid-vapor regime, if any, is small and the corresponding size of the critical nucleus of gas therefore large; consequently, too little translational energy is available to initiate bubble nucleation in the metastable region (see Sec. III C). (b) In this context, explosive boiling is expected to follow from highly localized *thermal* fluctuations in the superheated melt. Here, however, *thermal conduction* takes place on a shorter time scale and the system (locally) is, rather, efficiently cooled along the binodal: i.e., *phase explosion does not take place*. This strongly suggests equilibration of metallic liquids with their vapor in a time of $\sim10^{-11}$–10^{-10} s, with equally important consequences for the mechanisms of matter removal under nanosecond irradiation (see Sec. IV C).

Solidification of the nonablated molten material to a glass is eventually observed near the surface on a 10^{-10} s time scale ($D\rightarrow E$); closer to the solid-liquid interface [Fig. 14(b)], the metallic melt heterogeneously solidifies, instead, to a crystal (F) with a corresponding maximum regrowth velocity of $\approx$15 m s^{-1} (see Sec. III A 3).

B. Dynamics under supercritical expansion

As shown in Fig. 14(c), only those regions of the target expanding *above* the critical point contribute to the ablated mass. This is indicated by the split of the dense and macroscopic branches in the *single-phase*, supercritical region of the phase diagram (G); evaporation from the surface of the clusters produced in the dissociation process is responsible for the concomitant appearance of a gas branch. The further separation of the dense and macroscopic branches ($G\rightarrow H$), on the one hand, and the cooling of the condensed ($G\rightarrow I$) and gaseous (J) phases toward the binodal, on the other hand, are associated at later times with expansion and liquid-vapor equilibration within the plume, respectively.

In the present case, material removal does not result from the nucleation of a large, localized cavity in a subcritical, superheated liquid. Instead, ablation follows from the breakup of *supercritical* matter whereby voids initially develop *homogeneously* across the expanding material [Fig. 13(e)]; consequently, the ablating fluid does *not* exhibit a bubblelike character but, rather, a clusterlike, diffuse structure [Figs. 4(h) and 13(f)] very similar to that observed under far-from-threshold femtosecond irradiation [Fig. 4(g)].

Unquestionably, matter removal, which takes place *outside* of any phase coexistence region, cannot be ascribed to a phase transition such as, e.g., phase explosion or spinodal decomposition; "nontrivial" fragmentation of the irradiated material is also excluded in view of the relatively low expansion rate involved in the ejection process. However, it is well

established that a supercritical fluid at *equilibrium* and moderately low densities is *not* homogeneous.[74] In this regard, ablation under long, picosecond pulses can be described by a "trivial" fragmentation process:[75–77] the system—locally near thermodynamic equilibrium—undergoing slow expansion in vacuum reaches a region of the phase diagram [marked *G* in Fig. 14(c)] where the corresponding (equilibrium) structure is *not* that of a homogeneous fluid but, instead, corresponds to a collection of disconnected liquid droplets.

The nonablated molten matter solidifies at later times and the final structure is characterized by a ten-nanometer-thick layer of "frozen" liquid (glass) on top of a crystalline bulk material [Figs. 13(g) and 13(h)].

Note finally that: (i) The above behavior under picosecond irradiation has been observed at *all* fluences and for *each* of the pulse durations (ranging from 25 to 100 ps) investigated in this work;[76,77,148] similar conclusions have also been reported in metallic systems.[75] This suggests common pathways to matter removal in absorbing solids extending to picosecond and, possibly, nanosecond pulses. (ii) As mentioned earlier, the liquid-vapor region is *not* accessed in the picosecond regime; this implies a pulse duration upper limit for phase explosion of $\sim 10^{-11}-10^{-10}$ s. (iii) In view of the above discussion, the threshold for matter removal under picosecond pulses is determined by the minimum fluence at which *supercritical* expansion takes place. (iv) The ablation threshold *irradiance* for a 100 ps pulse is about 100 times *lower* than that observed for a 500 fs pulse; this can be explained by a significantly larger proportion of the laser energy which is absorbed via inverse bremsstrahlung (whereby the photon energy is entirely converted into kinetic energy of the carriers) in the metallic melt under picosecond irradiation.

C. Summary of thermodynamics under pulsed laser irradiation

In a paper published some thirty years ago,[69] Martynyuk pointed out that the total ablated mass and the liquid (not gaseous) character of the ejected material under relatively long ($\sim 10^{-7}-10^{-5}$ s) laser pulses cannot be explained by a simple evaporation model; prompted by this question, Martynyuk proposed a picture whereby the metallic liquid at undersaturated pressure undergoes a phase-explosion process as it is *rapidly heated into the liquid-vapor regime*.[69,85,86] The model, reintroduced a decade ago by Miotello and Kelly[70] for nanosecond pulses (and discussed at length in Sec. I), has since been put forward by numerous other authors for femtosecond to nanosecond pulses.[61,62,64–66,71,72,87,88]

However, the above (hypothetical) scenario is not supported by the thermodynamic pathways presented in Secs. III and IV. In this respect, Fig. 15 summarizes the thermodynamic routes observed in silicon under femtosecond and picosecond laser irradiation and illustrates the expected trajectory under longer, nanosecond pulses:

(i) Under femtosecond irradiation above the threshold fluence for ablation [Fig. 15(a)], the material is initially pulled

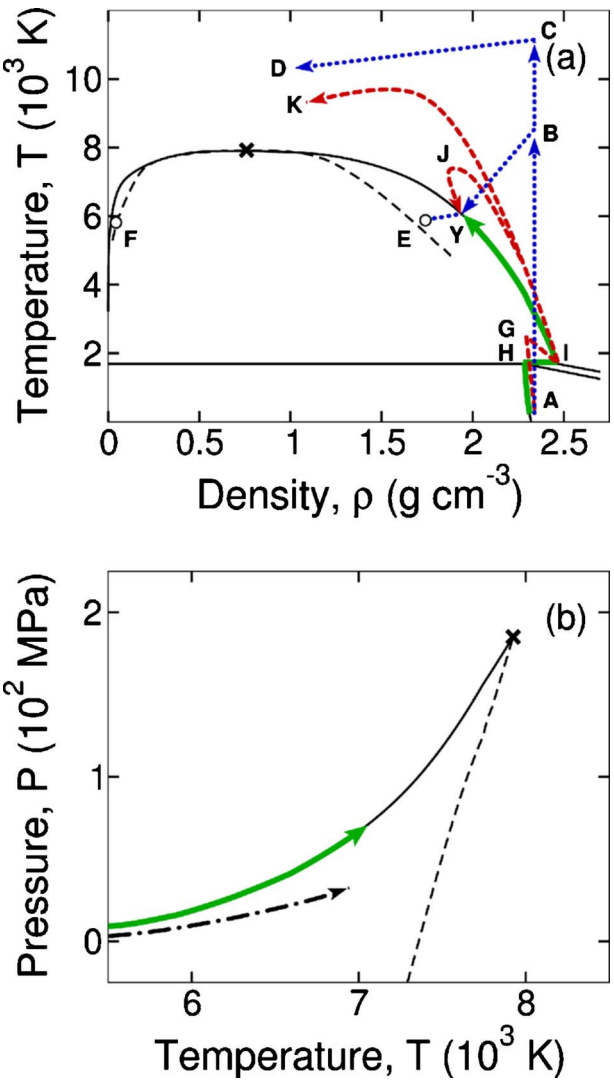

FIG. 15. (Color online) Schematic illustration of the thermodynamic pathways in silicon under femtosecond (blue dotted line), picosecond (red dashed line), and nanosecond (thick green solid line) irradiation: (a) ρ-T plane; (b) T-P plane. Capital letters refer to locations in the phase diagram (see text).

away from the liquid-vapor regime to a near-critical (marked $A \rightarrow B$) or supercritical ($A \rightarrow C$) state following mechanical instability in the strongly superheated solid and subsequent isochoric heating of the liquid: (a) In the former case, rapid adiabatic *cooling* of the system into the metastable region gives rise to a phase explosion of the subcritical, *superheated* liquid at a temperature significantly below $0.9T_c$ and in a time $\tau_{\mathrm{NUC}} \sim 10^{-12}-10^{-11}$ s ($B \rightarrow Y \rightarrow E \rightarrow F$). (b) In the latter case, the higher pressure gradient at the surface results in a faster, *supercritical* expansion of the initially homogeneous material which undergoes a *nonequilibrium* transition to a heterogeneous, clustered fluid through a "nontrivial" fragmentation process ($C \rightarrow D$).

(ii) Under picosecond irradiation, homogeneous and, at later times, heterogeneous melting of the superheated crystal ($A \rightarrow G \rightarrow I$) is followed by nonisochoric heating of the metallic melt. Here, the *subcritical* liquid material is eventually cooled along the binodal by heat conduction on a

$10^{-11}-10^{-10}$ s time scale and phase explosion does *not* take place ($I \rightarrow J \rightarrow Y$); as a result, matter removal is associated with the *near-equilibrium* expansion and dissociation into liquid droplets of *supercritical* matter undergoing a "trivial" fragmentation process ($I \rightarrow K$).

(iii) As the pulse duration τ_L is further increased, the solid-to-liquid transition is eventually expected to occur at the equilibrium melting temperature ($A \rightarrow H \rightarrow I$).[29,30] If $\tau_L \lesssim \tau_{\mathrm{LV}}$, where it is usually assumed that the liquid-vapor equilibration time $\tau_{\mathrm{LV}} \sim 10^{-9}-10^{-8}$ s,[64] the resulting heated liquid metal at undersaturated pressure will enter the metastable region [trajectory indicated by the dashed-dotted line in Fig. 15(b)] where explosive boiling may subsequently occur near the spinodal. However, the absence of *superheated liquid* states observed under picosecond irradiation suggests, rather, that $\tau_{\mathrm{LV}} \sim 10^{-11}-10^{-10}$ s. Consequently, it is more likely that heating takes place *along* the binodal under nanosecond pulses ($I \rightarrow Y$) [see also Fig. 15(b)].

In this case, the presence of large, micron-sized liquid droplets[94] in the plume could be explained by a second-order phase transition at the critical point near which the metallic melt is expected to transform into a dielectric;[17] hydrodynamic mechanisms could also account for the massive matter removal observed in the nanosecond regime.[149]

V. CONCLUSIONS AND FUTURE PERSPECTIVES

In conclusion, we have explored the thermodynamics involved in laser irradiation of silicon by 500 fs to 100 ps laser pulses. Our combined Monte Carlo and molecular-dynamics simulations reveal thermal transitions taking place between order and disorder and among different states of aggregation on mesoscopic-length and picosecond-to-nanosecond-time scales.

Upon femtosecond irradiation relatively far from the melting threshold, we observe the thermal disordering of a mechanically unstable solid in a time of $\sim 10^{-12}$ s. Under lower superheating with picosecond pulses, rapid homogeneous nucleation of liquid in the metastable solid is followed by slower, heterogeneous melting of the crystal. In contrast, solidification of the nonablated, supercooled melt to a crystal or a glass is a relatively slow process occurring on a $\sim 10^{-11}-10^{-9}$ s time scale, independent of the pulse duration.

At fluences above a well-defined threshold, hot, liquid material is ejected from the surface with a velocity of $\sim 10^2-10^3$ m s^{-1}. Under near-threshold irradiation with femtosecond pulses, the subcritical material undergoes rapid adiabatic cooling to the liquid-gas regime where a phase-explosion-like process takes place on a $10^{-12}-10^{-11}$ s time scale: here, the onset of ablation, determined by the growth of critical nuclei of the stable vapor phase in the metastable liquid phase, is *not* initiated by large, localized, thermal fluctuations but, rather, by a direct conversion of translational, *mechanical* energy into surface energy. At higher fluences, however, a *nonequilibrium* transition from a homogeneous supercritical fluid to a heterogeneous, clustered phase upon rapid expansion in vacuum, i.e., "nontrivial" fragmentation, determines the early stages of matter removal; recent experimental investigation of silicon nanoparticle generation via femtosecond laser ablation in vacuum supports this scenario.[23]

Under slower expansion with picosecond pulses, liquid-vapor equilibrium is achieved through efficient, nonadiabatic cooling of the *subcritical* liquid material onto the binodal: in this case, the system does *not* access the region of metastable states and phase explosion does *not* occur; as a result, ablation is associated with a "trivial" fragmentation process, i.e., a *near-equilibrium* transition from a homogeneous *supercritical* state to a heterogeneous, fragmented fluid upon relatively slow dilution in vacuum. This implies the equilibration of the metallic liquid with its vapor on a $\sim 10^{-11}-10^{-10}$ s time scale, thereby indicating a heating process *along* the binodal under nanosecond irradiation.

In view of similar conclusions for metallic systems,[74,75,77] this suggests universal routes to matter removal extending to pulse durations far beyond the femtosecond regime in absorbing solids;[13,98] in particular, the irrelevance of explosive boiling to picosecond and nanosecond laser irradiation should manifest itself by the absence of interference fringes (Newton rings) in ultrafast time-resolved optical-microscopy experiments.[80]

As a final note, the recent emergence of attosecond pulses is likely to push laser material processing toward new frontiers and horizons in the years to come:[150–152] in the same way that femtosecond lasers have revealed the existence of ultrafast, nonthermal phenomena following their advent in the early 1980s, the availability of attosecond pulses may unveil unexplored pathways where nonthermal effects are expected to play a greater role. In this regard, ultrashort electron and free-electron-laser x-ray pulses appear as promising candidates to probe new, extreme states of matter.[153]

ACKNOWLEDGMENTS

We are greatly indebted to Danny Perez for numerous fruitful discussions. P.L. also wishes to thank Philippe Beaucage, Paul Callan, Massimo V. Fischetti, Richard Leonelli, Ralf Meyer, Pier Luigi Silvestrelli, Klaus Sokolowski-Tinten, Frank H. Stillinger, Razvan Stoian, Henry M. van Driel, Dietrich von der Linde, and Leonid V. Zhigilei for their help and useful insights. This work has been supported by grants from the Natural Sciences and Engineering Research Council of Canada (NSERC), the Canada Research Chair on Laser Micro/Nano-engineering of Materials, and the *Fonds Québécois de la Recherche sur la Nature et les Technologies* (FQRNT). We are grateful to the *Réseau Québécois de Calcul de Haute Performance (RQCHP) for generous allocations of computer resoruces.*

*Electronic address: Laurent.Lewis@UMontreal.CA; url: http://www.esi.umontreal.ca/~grofnum/
†Electronic address: Michel.Meunier@polymtl.ca; url: http://lpl.phys.polymtl.ca/

[1] A. M. Lindenberg, J. Larsson, K. Sokolowski-Tinten, K. J. Gaffney, C. Blome, O. Synnergren, J. Sheppard, C. Caleman, A. G. MacPhee, D. Weinstein *et al.*, Science **308**, 392 (2005).
[2] K. Sokolowski-Tinten, C. Blome, J. Blums, A. Cavalleri, C. Dietrich, A. Tarasevitch, I. Uschmann, E. Förster, M. Kammler, M. Horn-von-Hoegen *et al.*, Nature (London) **422**, 287 (2003).
[3] A. Rousse, C. Rischel, S. Fourmaux, I. Uschmann, S. Sebban, G. Grillon, Ph. Balcou, E. Förster, J. P. Geindre, P. Audebert *et al.*, Nature (London) **410**, 65 (2001).
[4] B. J. Siwick, J. R. Dwyer, R. E. Jordan, and R. J. D. Miller, Science **302**, 1382 (2003).
[5] C. W. Siders, A. Cavalleri, K. Sokolowski-Tinten, Cs. Tóth, T. Guo, M. Kammler, M. Horn von Hoegen, K. R. Wilson, D. von der Linde, and C. P. J. Barty, Science **286**, 1340 (1999).
[6] S. K. Sundaram and E. Mazur, Nat. Mater. **1**, 217 (2002).
[7] N. Bloembergen, Rev. Mod. Phys. **71**, S283 (1999).
[8] See, e. g., M. von Allmen and A. Blatter, *Laser-Beam Interactions with Materials*, 2nd edition (Springer, Berlin, 1995).
[9] A. Cavalleri, Cs. Tóth, C. W. Siders, J. A. Squier, F. Ráksi, P. Forget, and J. C. Kieffer, Phys. Rev. Lett. **87**, 237401 (2001).
[10] K. Sokolowski-Tinten, C. Blome, C. Dietrich, A. Tarasevitch, M. Horn von Hoegen, D. von der Linde, A. Cavalleri, J. Squier, and M. Kammler, Phys. Rev. Lett. **87**, 225701 (2001).
[11] P. H. Bucksbaum and J. Bokor, Phys. Rev. Lett. **53**, 182 (1984).
[12] M. O. Thompson, J. W. Mayer, A. G. Cullis, H. C. Webber, N. G. Chew, J. M. Poate, and D. C. Jacobson, Phys. Rev. Lett. **50**, 896 (1983).
[13] K. Sokolowski-Tinten, J. Bialkowski, A. Cavalleri, D. von der Linde, A. Oparin, J. Meyer-ter-Vehn, and S. I. Anisimov, Phys. Rev. Lett. **81**, 224 (1998).
[14] V. V. Zhakhovskiĭ, K. Nishihara, S. I. Anisimov, and N. A. Inogamov, JETP Lett. **71**, 167 (2000).
[15] N. A. Inogamov, Yu. V. Petrov, S. I. Anisimov, A. M. Oparin, N. V. Shaposhnikov, D. von der Linde, and J. Meyer-ter-Vehn, JETP Lett. **69**, 310 (1999).
[16] J. M. Liu, A. M. Malvezzi, and N. Bloembergen, Appl. Phys. Lett. **49**, 622 (1986).
[17] V. A. Batanov, F. V. Bunkin, A. M. Prokhorov, and V. B. Fedorov, Sov. Phys. JETP **36**, 311 (1973).
[18] A. Borowiec, D. M. Bruce, D. T. Cassidy, and H. K. Haugen, Appl. Phys. Lett. **83**, 225 (2003).
[19] W. Zapka, W. Ziemlich, and A. C. Tam, Appl. Phys. Lett. **58**, 2217 (1991).
[20] J.-N. Gillet, J.-Y. Degorce, and M. Meunier, Appl. Phys. Lett. **86**, 222104 (2005).
[21] S. R. Shinde, S. B. Ogale, R. L. Greene, T. Venkatesan, P. C. Canfield, S. L. Bud'ko, G. Lapertot, and C. Petrovic, Appl. Phys. Lett. **79**, 227 (2001).
[22] P. R. Willmott and J. R. Huber, Rev. Mod. Phys. **72**, 315 (2000).
[23] S. Amoruso, R. Bruzzese, N. Spinelli, R. Velotta, M. Vitiello, X. Wang, G. Ausanio, V. Iannotti, and L. Lanotte, Appl. Phys. Lett. **84**, 4502 (2004).
[24] S. Amoruso, G. Ausanio, R. Bruzzese, M. Vitiello, and X. Wang, Phys. Rev. B **71**, 033406 (2005).
[25] J.-P. Sylvestre, A. V. Kabashin, E. Sacher, M. Meunier, and J. H. T. Luong, J. Am. Chem. Soc. **126**, 7176 (2004).
[26] A. Vogel and V. Venugopalan, Chem. Rev. (Washington, D.C.) **103**, 577 (2003).
[27] Y. Siegal, E. N. Glezer, L. Huang, and E. Mazur, Annu. Rev. Mater. Sci. **25**, 223 (1995).
[28] D. von der Linde, K. Sokolowski-Tinten, and J. Bialkowski, Appl. Surf. Sci. **109–110**, 1 (1997).
[29] N. Fabricius, P. Hermes, D. von der Linde, A. Pospieszczyk, and B. Stritzker, Solid State Commun. **58**, 239 (1986).
[30] D. von der Linde, in *Resonances: A Volume in Honor of the 70th Birthday of Nicolaas Bloembergen*, edited by M. D. Levenson, E. Mazur, P. S. Pershan, and Y. R. Shen (World Scientific Publishing, Singapore, 1991), pp. 337–347.
[31] S. I. Anisimov, B. L. Kapeliovich, and T. L. Perel'man, Sov. Phys. JETP **39**, 375 (1974).
[32] D. von der Linde and K. Sokolowski-Tinten, Appl. Surf. Sci. **154–155**, 1 (2000).
[33] B. Rethfeld, K. Sokolowski-Tinten, D. von der Linde, and S. I. Anisimov, Phys. Rev. B **65**, 092103 (2002).
[34] S. I. Ashitkov, M. B. Agranat, P. S. Kondratenko, S. I. Anisimov, V. E. Fortov, V. V. Temnov, K. Sokolowski-Tinten, B. Rethfeld, P. Zhou, and D. von der Linde, JETP Lett. **76**, 461 (2002).
[35] D. S. Ivanov and L. V. Zhigilei, Phys. Rev. Lett. **91**, 105701 (2003).
[36] D. S. Ivanov and L. V. Zhigilei, Phys. Rev. B **68**, 064114 (2003).
[37] S. I. Anisimov, N. A. Inogamov, A. M. Oparin, B. Rethfeld, T. Yabe, M. Ogawa, and V. E. Fortov, Appl. Phys. A **69**, 617 (1999).
[38] A. Cavalleri, K. Sokolowski-Tinten, J. Bialkowski, M. Schreiner, and D. von der Linde, J. Appl. Phys. **85**, 3301 (1999).
[39] S. M. Wiggins, J. Solis, and C. N. Afonso, Appl. Phys. Lett. **84**, 4445 (2004).
[40] P. L. Liu, R. Yen, N. Bloembergen, and R. T. Hodgson, Appl. Phys. Lett. **34**, 864 (1979).
[41] S. R. Stiffler, M. O. Thompson, and P. S. Peercy, Phys. Rev. Lett. **60**, 2519 (1988).
[42] B. C. Larson, J. Z. Tischler, and D. M. Mills, Mater. Res. Soc. Symp. Proc. **51**, 113 (1985).
[43] L. Huang, J. P. Callan, E. N. Glezer, and E. Mazur, Phys. Rev. Lett. **80**, 185 (1998).
[44] P. Saeta, J.-K. Wang, Y. Siegal, N. Bloembergen, and E. Mazur, Phys. Rev. Lett. **67**, 1023 (1991).
[45] K. Sokolowski-Tinten, J. Bialkowski, and D. von der Linde, Phys. Rev. B **51**, 14186 (1995).
[46] C. V. Shank, R. Yen, and C. Hirlimann, Phys. Rev. Lett. **50**, 454 (1983).
[47] P. L. Silvestrelli, A. Alavi, M. Parrinello, and D. Frenkel, Phys. Rev. Lett. **77**, 3149 (1996).
[48] K. Sokolowski-Tinten and D. von der Linde, Phys. Rev. B **61**, 2643 (2000).
[49] P. Stampfli and K. H. Bennemann, Phys. Rev. B **49**, 7299 (1994).
[50] In fact, the resulting molten structure is initially characterized by a higher coordination (between 11 and 13) and significantly reduced covalent-bonding attributes. However, this phase is only short-lived and the system rapidly assumes the usual properties of liquid silicon (Ref. 47).
[51] The picture of bond breaking and lattice collapse on ultrashort time scales does not apply to metals where cohesion of the close-packed structure is ensured by delocalized conduction electrons (Ref. 4). Instead, melting is strictly thermal and whether the liquid phase originates from a heterogeneous or ho-

mogeneous nucleation process depends on various parameters such as pulse duration and fluence (Refs. 35 and 36).
[52] B. Rethfeld, Phys. Rev. Lett. **92**, 187401 (2004).
[53] D. von der Linde and H. Schüler, J. Opt. Soc. Am. B **13**, 216 (1996).
[54] K. Sokolowski-Tinten, J. Bialkowski, A. Cavalleri, M. Boing, H. Schüler, and D. von der Linde, in *High Power Laser Ablation*, edited by C. R. Phipps (1998), Vol. 3343 of Proc. SPIE, pp. 46–57.
[55] D. von der Linde (private communication).
[56] R. Stoian, A. Rosenfeld, D. Ashkenasi, I. V. Hertel, N. M. Bulgakova, and E. E. B. Campbell, Phys. Rev. Lett. **88**, 097603 (2002).
[57] N. M. Bulgakova, R. Stoian, A. Rosenfeld, I. V. Hertel, and E. E. B. Campbell, Phys. Rev. B **69**, 054102 (2004).
[58] W. G. Roeterdink, L. B. F. Juurlink, O. P. H. Vaughan, J. Dura Diez, M. Bonn, and A. W. Kleyn, Appl. Phys. Lett. **82**, 4190 (2003).
[59] Conflicting views regarding the relevance of Coulomb explosion to semiconductors and metals, where the higher electron mobilities and densities would ensure an effective screening of the net positive charge at the surface, can be found in the literature [R. Stoian, A. Rosenfeld, I. V. Hertel, N. M. Bulgakova, and E. E. B. Campbell, Appl. Phys. Lett. **85**, 694 (2004); W. G. Roeterdink, M. Bonn, and A. W. Kleyn, Appl. Phys. Lett. **85**, 696 (2004)]. Nevertheless, if nonthermal melting of a highly excited semiconductor lattice (such as silicon) can be triggered *during* the pulse using, e.g., very high intensities, one can envisage that part of the laser radiation may interact with the metallic liquid phase, with significantly lower electron mobility (Ref. 109), to induce electrostatic charging and ablation at the surface (Ref. 154); this, however, has yet to be confirmed.
[60] B. N. Chichkov, C. Momma, S. Nolte, F. von Alvensleben, and A. Tünnermann, Appl. Phys. A **63**, 109 (1996).
[61] D. A. Willis and X. Xu, Appl. Surf. Sci. **197–198**, 118 (2002).
[62] D. A. Willis and X. Xu, Int. J. Heat Mass Transfer **45**, 3911 (2002).
[63] J. Jandeleit, G. Urbasch, H. D. Hoffmann, H.-G. Treusch, and E. W. Kreutz, Appl. Phys. A **63**, 117 (1996).
[64] N. M. Bulgakova and A. V. Bulgakov, Appl. Phys. A **73**, 199 (2001).
[65] K. H. Song and X. Xu, Appl. Surf. Sci. **127–129**, 111 (1998).
[66] J. H. Yoo, S. H. Jeong, X. L. Mao, R. Greif, and R. E. Russo, Appl. Phys. Lett. **76**, 783 (2000).
[67] To our knowledge, there has been no report of laser-induced optical breakdown in metals.
[68] Note that photochemical pathways involving the direct photodissociation of molecular bonds have also been proposed in organic solids [Y. G. Yingling and B. J. Garrison, Chem. Phys. Lett. **364**, 237 (2002)].
[69] M. M. Martynyuk, Sov. Phys. Tech. Phys. **21**, 430 (1976).
[70] A. Miotello and R. Kelly, Appl. Phys. Lett. **67**, 3535 (1995).
[71] L. V. Zhigilei and B. J. Garrison, J. Appl. Phys. **88**, 1281 (2000).
[72] C. Cheng and X. Xu, Phys. Rev. B **72**, 165415 (2005).
[73] D. Perez and L. J. Lewis, Phys. Rev. Lett. **89**, 255504 (2002).
[74] D. Perez and L. J. Lewis, Phys. Rev. B **67**, 184102 (2003).
[75] D. Perez and L. J. Lewis, Appl. Phys. A **79**, 987 (2004).
[76] P. Lorazo, L. J. Lewis, and M. Meunier, Phys. Rev. Lett. **91**, 225502 (2003).
[77] P. Lorazo, D. Perez, L. J. Lewis, and M. Meunier, in *High Power Laser Ablation V*, edited by C. R. Phipps (2004), Vol. 5448 of Proc. SPIE, pp. 520–531.
[78] F. Vidal, T. W. Johnston, S. Laville, O. Barthélemy, M. Chaker, B. Le Drogoff, J. Margot, and M. Sabsabi, Phys. Rev. Lett. **86**, 2573 (2001).
[79] P. P. Pronko, S. K. Dutta, D. Du, and R. K. Singh, J. Appl. Phys. **78**, 6233 (1995).
[80] S. I. Anisimov, V. V. Zhakhovskiĭ, N. A. Inogamov, K. Nishihara, A. M. Oparin, and Yu. V. Petrov, JETP Lett. **77**, 606 (2003).
[81] A. A. Oraevsky, S. L. Jacques, and F. K. Tittel, J. Appl. Phys. **78**, 1281 (1995).
[82] O. Yavas, P. Leiderer, H. K. Park, C. P. Grigoropoulos, C. C. Poon, and A. C. Tam, Phys. Rev. Lett. **72**, 2021 (1994).
[83] T. E. Glover, J. Opt. Soc. Am. B **20**, 125 (2003).
[84] A. Miotello and R. Kelly, Appl. Phys. A **69**, S67 (1999).
[85] M. M. Martynyuk, Russ. J. Phys. Chem. **57**, 494 (1983).
[86] M. M. Martynyuk, Sov. Phys. Tech. Phys. **19**, 793 (1974).
[87] J. K. Chen and J. E. Beraun, J. Opt. A, Pure Appl. Opt. **5**, 168 (2003).
[88] L. V. Zhigilei, E. Leveugle, B. J. Garrison, Y. G. Yingling, and M. I. Zeifman, Chem. Rev. (Washington, D.C.) **103**, 321 (2003).
[89] V. P. Carey, *Liquid-Vapor Phase-Change Phenomena* (Hemisphere, New York, 1992).
[90] In view of a number of experimental and computational studies suggesting the relevance of phase explosion to femtosecond (and picosecond) pulses, Miotello and Kelly later discarded the value of τ_{NUC} originally proposed by Martynyuk (Ref. 94).
[91] A. Cavalleri, K. Sokolowski-Tinten, J. Bialkowski, and D. von der Linde, Appl. Phys. Lett. **72**, 2385 (1998).
[92] X. Xu, Appl. Surf. Sci. **197–198**, 61 (2002).
[93] See also Ref. 94 and references therein.
[94] R. Kelly and A. Miotello, Phys. Rev. E **60**, 2616 (1999).
[95] Q. Lu, S. S. Mao, X. Mao, and R. E. Russo, Appl. Phys. Lett. **80**, 3072 (2002).
[96] B. J. Garrison, T. E. Itina, and L. V. Zhigilei, Phys. Rev. E **68**, 041501 (2003).
[97] N. A. Inogamov, S. I. Anisimov, and B. Retfeld, J. Exp. Theor. Phys. **88**, 1143 (1999).
[98] B. Rethfeld, V. V. Temnov, K. Sokolowski-Tinten, S. I. Anisimov, and D. von der Linde, in *High Power Laser Ablation IV*, edited by C. R. Phipps (2002), Vol. 4760 of Proc. SPIE, pp. 72–80.
[99] See, e.g., F. Bassani and G. Pastori Parravicini, *Electronic States and Optical Transitions in Solids* (Pergamon Press, Oxford, 1975).
[100] In the present study, the optical response of the irradiated material is dominated by linear processes and multiphoton transitions are ignored. This can be justified by estimating the value of $G_{12}(\mathbf{r}_i,t)=(1-R_i)I(\mathbf{r}_i,t)\beta(\mathbf{r}_i,t)/(2\alpha_i)$ which expresses the local ratio of the two-photon to the one-photon interband transition rates in the crystalline, semiconducting phase (Ref. 102). With $R_i \approx 0.7$ and $\alpha_i \approx 2\times 10^6\ \mathrm{cm}^{-1}$ (Ref. 155), $\beta(\mathbf{r}_i,t) \lesssim 40\ \mathrm{cm\,GW}^{-1}$ the two-photon absorption coefficient (Ref. 156), and an irradiance $I(\mathbf{r}_i,t) \lesssim 10^{12}\ \mathrm{W\,cm}^{-2}$ (see Sec. III), we have that $G_{12} \lesssim 10^{-3}$.
[101] The temperature dependence of $\epsilon_{\mathrm{vc}}^{*}$ has been obtained from a fit to the experimental data in Ref. 155.
[102] H. M. van Driel, Phys. Rev. B **35**, 8166 (1987).
[103] The overall changes to the dielectric constant due to state-and-band filling and band-structure renormalization are relatively small and are consequently neglected (Ref. 48).

[104] A Drude damping time $\tau_D=10$ fs and an optical effective mass $m^*_{\mathrm{opt}}=(m_e^{*-1}+m_h^{*-1})^{-1}=0.375m_e$ [where the electron and hole mobility effective masses m_e^* and m_h^* are equal to $0.75m_e$ (see Sec. II A 1)] are used in the solid phase, irrespective of the pulse duration; the values of τ_D and m^*_{opt} in the liquid phase have been taken from Ref. 105.
[105] K. D. Li and P. M. Fauchet, Appl. Phys. Lett. **51**, 1747 (1987).
[106] G. Gantner, H. G. Boyen, and P. Oelhafen, Europhys. Lett. **31**, 163 (1995).
[107] This is based upon the following two observations: (i) Because single-photon processes govern the optical response of the material (see note in Ref. 100), conduction-band electrons are initially generated in the crystal with a maximum kinetic energy $\hbar\omega_L-E_g\approx 3.5$ eV which is below the minimum energy required to escape the solid, as given by the electron affinity $\chi\approx 3.7$ eV [J. R. Goldman and J. A. Prybyla, Phys. Rev. Lett. **72**, 1364 (1994)]. (ii) A photon may excite a *conduction* electron above the vacuum level (since $\hbar\omega_L>\chi$), thus leaving the surface with a net positive charge; at sufficiently high irradiances, this could lead to space-charge effects which are not accounted for by our model. However, recent experiments and calculations have shown that such a positive charge would be rapidly balanced out by the diffusion of electrons from the bulk (Refs. 56 and 57). The same reasoning applies to thermionic emission which is also neglected.
[108] A. M. Malvezzi, J. M. Liu, and N. Bloembergen, Mater. Res. Soc. Symp. Proc. **23**, 135 (1984).
[109] V. M. Glazov and V. B. Kol'tsov, Sov. Phys. Semicond. **18**, 1153 (1984).
[110] M. Lundstrom, *Fundamentals of Carrier Transport*, 2nd edition (Cambridge University Press, Cambridge, 2000).
[111] C. Jacoboni and L. Reggiani, Rev. Mod. Phys. **55**, 645 (1983).
[112] Y. Kamakura, H. Mizuno, M. Yamaji, M. Morifuji, K. Taniguchi, C. Hamaguchi, T. Kunikiyo, and M. Takenaka, J. Appl. Phys. **75**, 3500 (1994).
[113] T. Kunikiyo, M. Takenaka, M. Morifuji, K. Taniguchi, and C. Hamaguchi, J. Appl. Phys. **79**, 7718 (1996).
[114] In the present model, carriers are not allowed to absorb phonons.
[115] See note in Ref. 107.
[116] Other phenomena, such as possible screening of the electron-phonon interaction [E. J. Yoffa, Phys. Rev. B **23**, 1909 (1981); T. Sjodin, H. Petek, and H.-L. Dai, Phys. Rev. Lett. **81**, 5664 (1998)], recombination at surface trap states [N. J. Halas and J. Bokor, Phys. Rev. Lett. **62**, 1679 (1989)], many-body effects [J. F. Young and H. M. van Driel, Phys. Rev. B **26**, 2147 (1982)], electron confinement due to band-gap shrinkage (Ref. 27), and scattering by ionized impurities or plasmons (Ref. 110), are ignored for simplicity.
[117] V. V. Godlevsky, J. J. Derby, and J. R. Chelikowsky, Phys. Rev. Lett. **81**, 4959 (1998).
[118] V. M. Glazov, S. N. Chizhevskaya, and N. N. Glagoleva, *Liquid Semiconductors* (Plenum Press, New York, 1969).
[119] P. Beaucage and N. Mousseau, Phys. Rev. B **71**, 094102 (2005).
[120] See, e. g., M. P. Allen and D. J. Tildesley, *Computer Simulation of Liquids* (Oxford University Press, Oxford, 1987).
[121] F. H. Stillinger and T. A. Weber, Phys. Rev. B **31**, 5262 (1985).
[122] J. C. Noya, C. P. Herrero, and R. Ramírez, Phys. Rev. B **53**, 9869 (1996).
[123] E. R. Cowley, Phys. Rev. Lett. **60**, 2379 (1988).
[124] J. Q. Broughton and X. P. Li, Phys. Rev. B **35**, 9120 (1987).
[125] F. F. Abraham and J. Q. Broughton, Phys. Rev. Lett. **56**, 734 (1986).
[126] H. Balamane, T. Halicioglu, and W. A. Tiller, Phys. Rev. B **46**, 2250 (1992).
[127] S. Sastry and C. A. Angell, Nat. Mater. **2**, 739 (2003).
[128] P. Beaucage and N. Mousseau, J. Phys.: Condens. Matter **17**, 2269 (2005).
[129] W. D. Luedtke and U. Landman, Phys. Rev. B **40**, 1164 (1989).
[130] J. Hoshen and R. Kopelman, Phys. Rev. B **14**, 3438 (1976).
[131] N. Honda and Y. Nagasaka, Int. J. Thermophys. **20**, 837 (1999).
[132] See, e.g., M. J. Moran and H. N. Shapiro, *Fundamentals of Engineering Thermodynamics*, 4th edition (John Wiley and Sons, New York, 2000).
[133] D. V. Makhov and L. J. Lewis, Phys. Rev. B **67**, 153202 (2003).
[134] S. W. Koch, R. C. Desai, and F. F. Abraham, Phys. Rev. A **27**, 2152 (1983).
[135] See, e.g., C. Kittel, *Introduction to Solid State Physics*, 8th edition (John Wiley and Sons, New York, 2005).
[136] M. D. Kluge and J. R. Ray, Phys. Rev. B **39**, 1738 (1989).
[137] R. Tsu, R. T. Hodgson, T. Y. Tan, and J. E. Baglin, Phys. Rev. Lett. **42**, 1356 (1979).
[138] A. G. Cullis, H. C. Webber, N. G. Chew, J. M. Poate, and P. Baeri, Phys. Rev. Lett. **49**, 219 (1982).
[139] R. F. Wood, Mater. Res. Soc. Symp. Proc. **13**, 83 (1983).
[140] C. Schäfer, H. M. Urbassek, and L. V. Zhigilei, Phys. Rev. B **66**, 115404 (2002).
[141] N. N. Nedialkov, S. E. Imamova, and P. A. Atanasov, J. Phys. D **37**, 638 (2004).
[142] L. V. Zhigilei, P. B. S. Kodali, and B. J. Garrison, Chem. Phys. Lett. **276**, 269 (1997).
[143] In metallic systems, *near*-threshold ablation is driven by spallation; at higher fluences, phase explosion and, eventually, fragmentation are responsible for matter removal (Ref. 74).
[144] As expected for a picosecond pulse, this is strictly below the critical electron density $N_c\approx 10^{22}$ cm^{-3} for nonthermal melting.
[145] See, e.g., Ref. 33 and references therein.
[146] In Ref. 147, z takes positive values and the temperature gradient is, instead, *positive*.
[147] K. Sokolowski-Tinten, J. Bialkowski, M. Boing, A. Cavalleri, and D. von der Linde, Phys. Rev. B **58**, R11805 (1998).
[148] In the case of a 5 ps pulse, near-threshold ablation involves, rather, a phase-explosion scenario (Ref. 76).
[149] L. V. Zhigilei, Appl. Phys. A **76**, 339 (2003).
[150] N. A. Papadogiannis, B. Witzel, C. Kalpouzos, and D. Charalambidis, Phys. Rev. Lett. **83**, 4289 (1999).
[151] P. M. Paul, E. S. Toma, P. Breger, G. Mullot, F. Augé, Ph. Balcou, H. G. Muller, and P. Agostini, Science **292**, 1689 (2001).
[152] M. Hentschel, R. Kienberger, Ch. Spielmann, G. A. Reider, N. Milosevic, T. Brabec, P. Corkum, U. Heinzmann, M. Drescher, and F. Krausz, Nature (London) **414**, 509 (2001).
[153] D. von der Linde, Science **302**, 1345 (2003).
[154] R. Stoian (private communication).
[155] B. K. Sun, X. Zhang, and C. P. Grigoropoulos, Int. J. Heat Mass Transfer **40**, 1591 (1997).
[156] M. Murayama and T. Nakayama, Phys. Rev. B **52**, 4986 (1995).